

RooflineBench: A Benchmarking Framework for On-Device LLMs via Roofline Analysis

Zhen Bi^{1,2*} Xueshu Chen^{1,2*} Luoyang Sun^{2,3} Yuhang Yao^{2,4} Qing Shen¹ Jungang Lou^{1,†} Cheng Deng^{2,5†}

Abstract

The transition toward localized intelligence through Small Language Models (SLMs) has intensified the need for rigorous performance characterization on resource-constrained edge hardware. However, objectively measuring the theoretical performance ceilings of diverse architectures across heterogeneous platforms remains a formidable challenge. In this work, we propose a systematic framework based on the Roofline model that unifies architectural primitives and hardware constraints through the lens of operational intensity (OI). By defining an inference-potential region, we introduce the *Relative Inference Potential* as a novel metric to compare efficiency differences between Large Language Models (LLMs) on the same hardware substrate. Extensive empirical analysis across diverse compute tiers reveals that variations in performance and OI are significantly influenced by sequence length. We further identify a critical regression in OI as model depth increases. Additionally, our findings highlight an efficiency trap induced by hardware heterogeneity and demonstrate how structural refinements, such as Multi-head Latent Attention (MLA), can effectively unlock latent inference potential across various hardware substrates. These insights provide actionable directions for hardware-software co-design to align neural structures with physical constraints in on-device intelligence. The released code is available in the Appendix C.

1. Introduction

The rapid advancement of Large Language Models (LLMs) has redefined the landscape of artificial intelligence, yet their

¹Huzhou University ²Banbu AI Foundation ³Institution of Automation, Chinese Academy of Sciences ⁴Carnegie Mellon University ⁵University of Edinburgh. Correspondence to: Jungang Lou and Cheng Deng <bizhen@zjhu.edu.cn | cdeng@ed.ac.uk>.

Preprint. February 13, 2026.

substantial scales continue to impose significant burdens on resource efficiency and deployment costs (Hoffmann et al., 2022). This challenge has catalyzed a paradigm shift toward Small Language Models (SLMs) that prioritize capacity density and on-device accessibility (Liu et al., 2024). Recent breakthroughs, including the Gemma, Phi-3, and MiniCPM families, demonstrate that compact architectures can rival significantly larger models while remaining deployable on consumer hardware (Team, 2024a; Abdin et al., 2024; Hu et al., 2024). This trajectory further extends to the multimodal domain, where efficient models like MiniCPM-V and LLaVA-v1.6 surpass proprietary counterparts with minimal computational overhead (Yao et al., 2024; Yu et al., 2025; Li et al., 2023). Such developments underscore a critical transition toward localized intelligence that ensures data privacy and democratizes powerful AI capabilities across edge devices.

Recent literature has increasingly prioritized the quantitative assessment of inference efficiency through specialized metrics such as Model Bandwidth Utilization (MBU) (Agarwal et al., 2023), Model FLOPs Utilization (MFU) (Chowdhery et al., 2023), and evaluation frameworks like MoeCap (Jiang et al., 2025). Despite these advancements, establishing a comprehensive understanding of on-device intelligence remains a formidable task. Primarily, objectively characterizing the theoretical performance upper bound for specific large model architectures when deployed on heterogeneous hardware platforms is challenging because of the complex interplay between software kernels and hardware substrates (Dao et al., 2022). Furthermore, conventional evaluation methods often lack the analytical depth required to pinpoint the fundamental physical constraints limiting inference efficacy in resource-constrained environments. These limitations necessitate a more robust analytical framework that can decompose hardware-software interactions to identify precise bottlenecks across diverse compute tiers.

To address these challenges, we leverage the Roofline model as a rigorous analytical bridge to characterize the interplay between large model inference and underlying hardware capabilities (Williams et al., 2009). Our approach entails the empirical measurement of peak $FLOPS$ and memory bandwidth to establish a realistic performance envelope

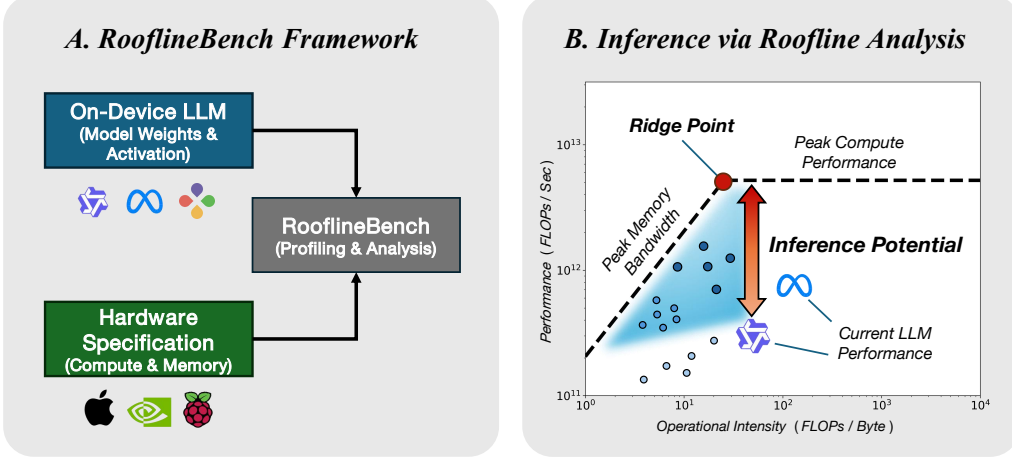


Figure 1. Overview of the RooflineBench framework and analytical methodology. **Left:** The integrated profiling system incorporating on-device LLM configurations and hardware specifications for systematic analysis. **Right:** Graphical representation of the Roofline model illustrating the *Relative Inference Potential* between observed throughput and theoretical hardware ceilings across both memory-bound and compute-bound regimes.

across diverse platforms. We also argue that LLMs exhibit an inference potential region on edge hardware devices (the blue region in Figure 1), and we propose a novel metric (*Relative Inference Potential*) to compare the differences in inference potential between two LLMs on the same hardware device. The primary contributions of this work are three fold:

- **Integrated Benchmarking Framework:** We propose a systematic Roofline based framework that unifies architectural primitives and hardware constraints via operational intensity (OI), defining an inference potential region to introduce the Relative Inference Potential (Φ) for comparative efficiency analysis.
- **Comprehensive Empirical Analysis:** Through extensive experiments across heterogeneous compute tiers, we reveal that inference efficiency is primarily governed by context length and attention architectures, while identifying a critical OI regression at increased model depths.
- **Hardware-Software Co-design Inspirations:** Our findings identify an efficiency trap induced by hardware heterogeneity and demonstrate how architectural refinements can maximize utilization across diverse hardware substrates to effectively bridge the gap between theoretical potential and real world execution.

2. Background

The Physics of On-Device Decoding Following the analytical framework of *Pope et al.* (Pope et al., 2023), we deconstruct Transformer inference into two phases: prefill

and decoding. While the prefill phase processes input tokens in parallel and is typically compute-bound, the decoding phase generates tokens autoregressively, where each step sequentially depends on previously generated tokens. This sequential nature inherently shifts the execution bottleneck toward memory bandwidth.

Mathematical Derivation of the Bandwidth Bottleneck

For a decoder-only model with n_{params} parameters, it has been shown that the forward pass requires approximately $2 \cdot n_{params}$ floating-point operations (FLOPs) per token. Let P_{peak} be the peak performance of the hardware and BW be the memory bandwidth. During decoding, the model weights and the attention key-value (KV) cache must be transferred from memory to compute cores for every single token. We define the *compute time* (T_{comp}) and *memory time* (T_{mem}) as:

$$T_{comp} = \frac{2 \cdot n_{params}}{P_{peak}} \quad (1)$$

$$T_{mem} \approx \frac{n_{params} \cdot b_{prec}}{BW} \quad (2)$$

where b_{prec} is the bytes per parameter. The system is memory-bandwidth bound when $T_{mem} > T_{comp}$. This constraint is captured by the *Operational Intensity* (OI):

$$OI_{dec} \approx \frac{2 \cdot n_{params}}{n_{params} \cdot b_{prec}} = \frac{2}{b_{prec}} \quad (3)$$

For 16-bit precision ($b_{prec} = 2$), $OI_{decode} \approx 1$ FLOP/Byte. Since modern edge accelerators often have P_{peak}/BW ratios far exceeding 1, the computational cores remain essentially idle while waiting for tensors to be loaded, leading to low model FLOPs utilization (MFU).

Edge Heterogeneity and KV Cache Scaling On resource-constrained edge devices, the additional memory traffic from the KV cache further reduces the system’s Operational Intensity (OI), shifting the execution point to the *left* on the Roofline model (Williams et al., 2009). Simultaneously, the limited memory bandwidth (BW) of mobile SoCs causes the hardware’s “knee point” (P_{peak}/BW) to shift to the *right*. This dual effect forces the decoding phase deep into the severe memory-bandwidth bound region, where the computational cores remain underutilized while waiting for tensor loading. Consequently, architectural optimizations such as multiquery attention (MQA) are essential to reduce the KV cache footprint and alleviate this bandwidth pressure.

3. Methodology: The Integrated Standard Roofline Framework

This section presents our performance analysis framework. Unlike simulation-based approaches, our tool is runtime-integrated, designed to quantify LLM’s inference potential by comparing real-time inference telemetry against empirically measured hardware limits.

3.1. Standard Roofline Formulation

We adopt the standard Roofline model to establish the theoretical performance upper bound. For a given hardware platform, attainable performance P (GFLOPS) is bounded by either compute capacity or memory bandwidth:

$$P = \min(P_{peak}, OI \times BW_{peak})$$

Where P_{peak} : Theoretical peak compute performance (GFLOPS). BW_{peak} : Achievable peak memory bandwidth (GB/s). OI (Operational Intensity): The ratio of floating-point operations to bytes of memory traffic (FLOPs/Byte). Given the autoregressive nature of LLM decoding (token-by-token generation), the process is inherently memory-bound. Consequently, our analysis focuses primarily on the **sloped region** of the Roofline graph, where performance is strictly limited by $OI \times BW_{peak}$.

3.2. Applying the Standard Roofline Model to LLMs

To rigorously quantify the efficiency of LLM decoding, we instantiate the Roofline model by defining its three core coordinates: theoretical FLOPs, memory traffic, and empirical hardware limits.

- **FLOPs (W): Analytical Estimation.** Directly measuring FLOPs via hardware counters can be imprecise due to instrumentation overhead. Instead, we adopt the analytical formulation from Sun et al. (2025) to estimate the theoretical FLOPs for heterogeneous architectures (e.g., MHA, GQA). Given a model with

hidden dimension H , sequence length N , and head configurations $\{n_q, n_k, n_v\}$, we precisely calculate the computational load for the Linear, Attention, and FFN layers per decoding step. This ensures a uniform standard for calculating Performance (P) and Operational Intensity (OI) across different backends.

- **Memory Traffic (Q): Data Movement Approximation.** In the context of memory-bound LLM decoding, memory traffic is dominated by loading model weights and the KV cache. We approximate the total data movement Q per token generation as the summation of the model parameters size and the active KV cache entries read/written during that step. This approach captures the requisite data transfer volume regardless of the specific memory management implementation (e.g., Unified Memory on Apple Silicon vs. GDDR6X on NVIDIA GPUs).

- **Performance & Operational Intensity Formulation.** Based on the derived W and Q , combined with the measured end-to-end latency (T), we define the runtime metrics as:

$$\text{Performance (GFLOPS)} = \frac{W}{T} \quad (4)$$

$$\text{Operational Intensity (FLOPs/Byte)} = \frac{W}{Q} \quad (5)$$

- **Hardware Limit Characterization.** We establish the theoretical ceiling by empirically profiling the peak memory bandwidth (BW_{peak}) and compute performance (P_{peak}). For Apple Silicon devices, we benchmark the Unified Memory bandwidth, as the GPU shares system memory. Conversely, for CUDA-enabled devices (e.g., RTX 4090), we isolate and measure the dedicated Video Memory (VRAM) bandwidth, as it constitutes the primary bottleneck for on-device inference.

3.3. Characterizing Relative Inference Potential across Performance Regimes

We define *Relative Inference Potential* (Φ) to quantify optimization headroom based on the spatial relationship between a performance point $P(OI_p, Perf_p)$ and the hardware ridge $R(OI_r, \pi)$. The calculation logic varies across different regimes to reflect shifting physical constraints.

Memory Bound Regime ($OI < OI_r$): Φ is the Euclidean distance to R , capturing the dual necessity of increasing operational intensity and throughput:

$$\Phi(P) = \sqrt{(OI_r - OI_p)^2 + (\pi - Perf_p)^2} \quad (6)$$

Compute Bound Regime ($OI \geq OI_r$): Since horizontal OI gains yield negligible ceiling increases, Φ is defined as

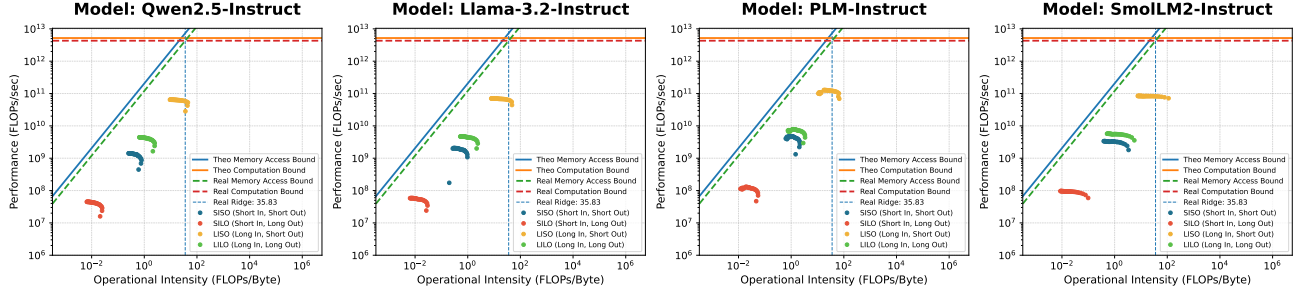


Figure 2. Comparison of roofline models across different input-output sequence length scenarios on Apple M1 Pro. Performance is evaluated in FP16 precision for Qwen2.5-Instruct (GQA), Llama-3.2-Instruct (GQA), PLM-Instruct (MLA), and SmoILM2-Instruct (MHA). The markers represent four inference scenarios: SISO, SILO, LISO, and LILO. Detailed analysis of the sensitivity to attention mechanisms is provided in subsequent sections. For comprehensive and detailed benchmarks across a wider range of hardware devices, please refer to Appendix D.

the vertical distance to the peak compute limit π :

$$\Phi(P) = \pi - \text{Perf}_p \quad (7)$$

Cross Regime Incomparability: Data points on opposite sides of the ridge are fundamentally incomparable due to distinct physical bottlenecks (bandwidth vs computation), necessitating regime specific evaluation.

4. Comprehensive Characterization Study

This section provides a systematic characterization of LLM inference using the proposed *Relative Inference Potential* (Φ) within a Roofline analytical framework. Unlike traditional macro metrics such as throughput (TPS), Φ facilitates a regime aware evaluation of execution efficiency by quantifying the spatial discrepancy between realized performance and theoretical hardware limits. We evaluate task level sensitivity across four sequence patterns (Sec. 4.1), investigate parameter level scaling and bottleneck shifts through model depth profiling (Sec. 4.2), and assess algorithmic impacts from precision and architectural refinements such as *MLA* (Sec. 4.3). **By identifying critical transitions between memory bound and compute bound regimes, this multi-dimensional analysis leverages Φ to reveal the internal complexity and optimization headroom of localized intelligence.** Experimental details are in Appendix C.

4.1. Sensitivity to Input-Output Sequence Lengths

To evaluate the impact of task-level workloads on on-device decoding efficiency, we categorize four representative sequence patterns based on typical edge-side use cases: (i) SISO (Short In, Short Out), such as local voice commands; (ii) SILO (Short In, Long Out), typical of creative writing or code completion; (iii) LISO (Long In, Short Out), reflecting RAG-based context extraction or document summarization; and (iv) LILO (Long In, Long Out), characteristic of document translation. These configurations fundamentally alter

the ratio between attention-related computation and model weight loading during each autoregressive step.

In Figure 2, decoding performance exhibits significant sensitivity to sequence lengths across all tested models. Notably, the LISO scenario (yellow dots) consistently achieves the highest execution efficiency, positioning itself as the closest observed case to the Roofline ridge point. This proximity stems from the larger input context, which increases the relative computational demand of the attention mechanism within each decoding step. By effectively amortizing the fixed memory overhead of loading model weights, LISO exhibits a high computational proportion, thereby elevating both the operational intensity (OI) and attainable performance ($GFLOPS$) toward the hardware’s compute-bound limit. Conversely, the SILO scenario (red dots) resides deep within the memory-bound regime. In this scenario, the negligible computational requirement of processing a minimal context cannot offset the massive data movement of weights, leading to severe hardware underutilization.

Insight.1. *Context length is the primary factor determining both the operational intensity and performance of on-device decoding: the LISO scenario approaches the compute-bound limit due to its inherently high computational proportion, while the SILO scenario remains severely memory-bound.*

4.2. Bottleneck Evolution under Parameter Expansion

To investigate the impact of model scale on on-device inference dynamics, we evaluate a series of configurations by scaling the number of Transformer layers from 2 to 64. This range encompasses both ultra-lightweight edge models and standard mobile-class LLMs, providing a continuous spectrum to observe performance scaling laws across varying parameter capacities.

As illustrated in Figure 3, scaling model depth reveals a dis-

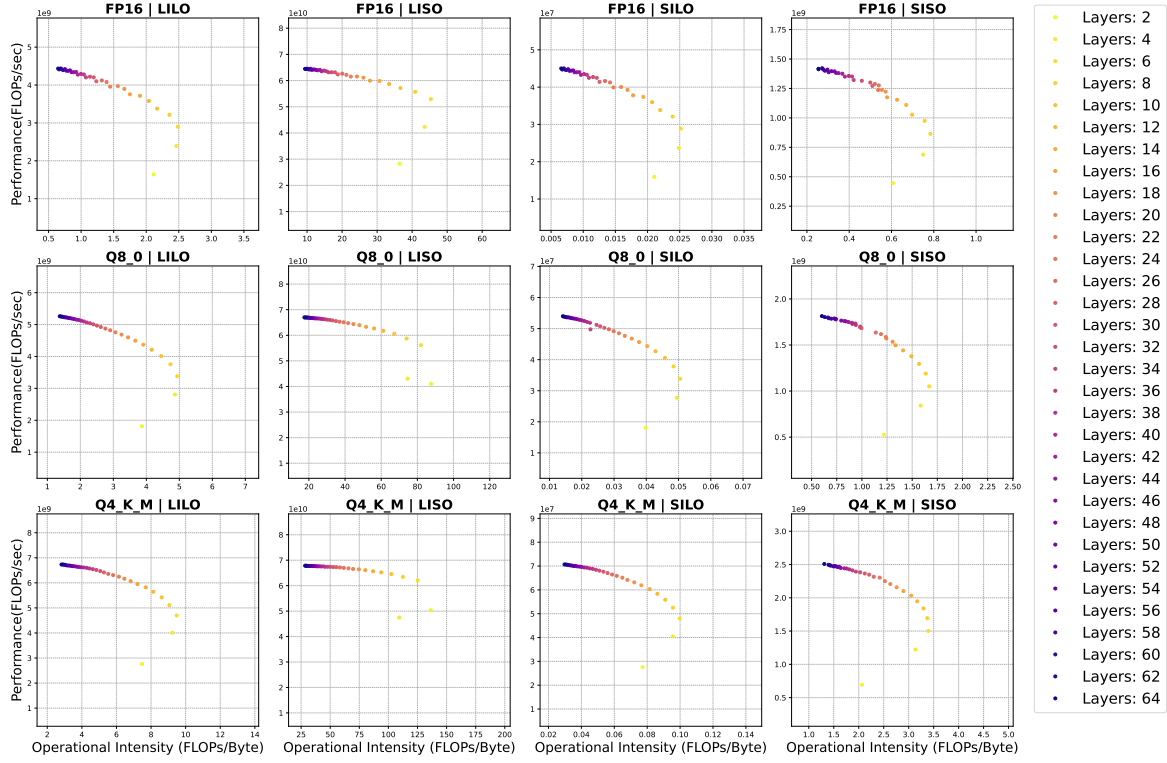


Figure 3. The figure shows the inference performance of Qwen2.5-Instruct FP16, Q8_0, and Q4_K_M with 2 to 64 layers (Experimental platform: Apple M1 Pro). Comprehensive and detailed benchmarks across a wider range of hardware devices are in Appendix D.

tinct, non-linear evolution of hardware utilization on edge platforms. Initially, the attainable performance ($GFLOPS$) rises consistently and becomes increasingly dense as layers increase (transitioning from light yellow to dark purple dots). This behavior suggests that deeper models more effectively amortize fixed system-level overheads—such as kernel launch latencies, memory synchronization, and command orchestration—thereby enabling the hardware to operate closer to its steady-state compute limits.

More significantly, the operational intensity (OI) exhibits a non-monotonic “arch” trajectory with a clear inflection point at remarkably shallow depths. As depth increases from 2 to approximately 3–5 layers, the data points initially shift to the right, indicating an initial gain in arithmetic reuse as the system moves away from the overhead-dominated regime. However, beyond this threshold, the OI begins to retreat to the left. In resource-constrained on-device environments, this regression arises because the cumulative memory bandwidth pressure of streaming weights for additional layers begins to outpace the marginal gains in computational reuse during the decoding phase. Consequently, the hardware “memory-wall” is encountered significantly earlier than theoretical predictions suggest, forcing the decoding process into an increasingly memory-bound regime as the model scales, which further constrains the release of relative inference-potential.

Insight.2. *On-device decoding reaches peak operational intensity at a remarkably shallow depth (3–5 layers), beyond which the memory bandwidth overhead of weight-streaming triggers a regression in operational intensity.*

4.3. Algorithmic Influences on Operational Intensity

Algorithmic optimizations fundamentally reshape the inference profile on the Roofline plane by modulating the balance between data movement and computation. This section evaluates the impact of numerical precision (Sec. 4.3.1) and attention architectures (Sec. 4.3.2) on the operational intensity (OI) and bottleneck transitions of on-device LLMs.

4.3.1. NUMERICAL PRECISION: FROM FP16 TO 4-BIT QUANTIZATION

To evaluate the impact of numerical precision on on-device efficiency, we compare FP16, Q8_0, and Q_K_M formats. Quantization directly reduces the memory footprint of model weights, fundamentally reshaping the data movement characteristics during edge deployment. Detailed FLOPs calculation formulas for the KV cache and attention mechanisms across these architectures are in Appendix C.

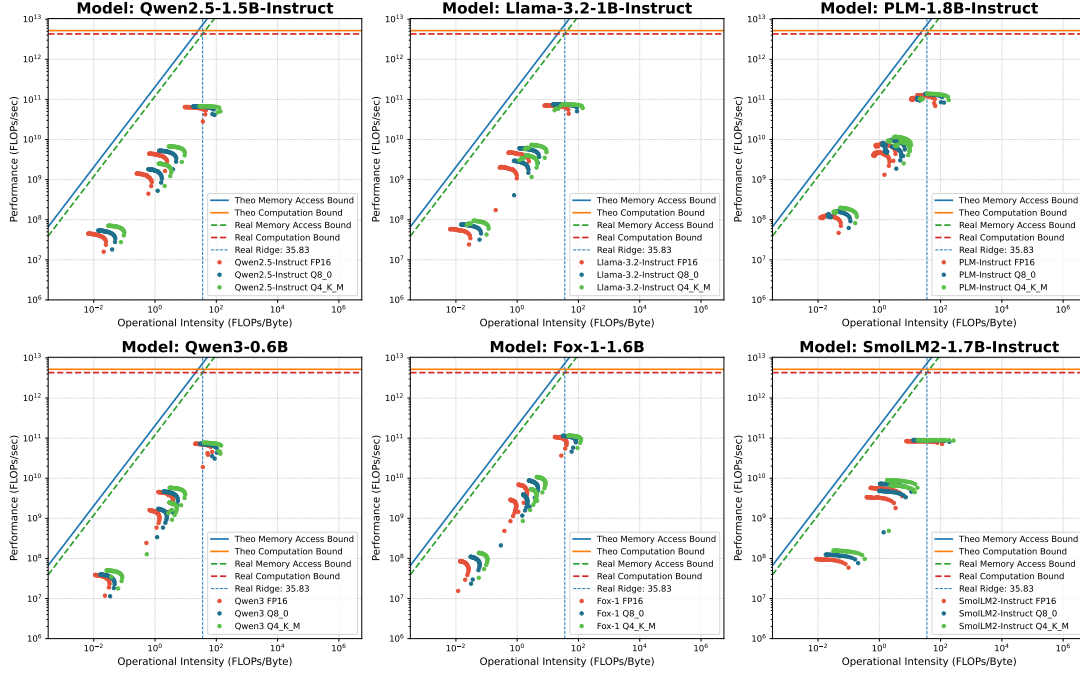


Figure 4. Performance comparison of various models across three different precision settings and all benchmarked hardware platforms. The results demonstrate a consistent performance gap and uniform trends, regardless of the specific device or precision level employed.

In Figure 4, lowering numerical precision triggers a diagonal shift of the data points toward the upper-right region of the Roofline plane. However, the magnitude of this improvement is highly sensitive to the task-level bottleneck. In memory-bound scenarios such as SILO (bottom-left), transitioning from FP16 to Q4_K_M yields dramatic gains in both operational intensity (OI) and attainable performance (*GFLOPS*), as the reduced bandwidth pressure directly accelerates the execution. Conversely, in the LISO scenario (top-right), the clusters for the three precisions appear significantly tighter. Since LISO is already positioned near the Roofline ridge with high arithmetic intensity, the benefits of reduced data movement are less pronounced, indicating that the execution has largely transitioned from being memory-constrained to being limited by the hardware’s peak compute capability.

Insight.3. *Quantization provides maximal efficiency gains for memory-bound tasks (e.g., SILO), whereas in compute-heavy scenarios (e.g., LISO), the performance becomes increasingly saturated as it approaches the hardware’s theoretical peak.*

4.3.2. ATTENTION MECHANISMS: MULTI-HEAD VS. SPARSE VARIATIONS

To investigate the impact of attention architectures on hardware efficiency, we compare three prevalent designs: Multi-Head Attention (MHA), Grouped-Query Attention (GQA) and Multi-head Latent Attention (MLA). To ensure fairness,

all LLMs are scaled to a unified size of approximately 1.5B parameters by adjusting their respective layer counts.

In Figure 6, the choice of attention mechanism significantly shifts the inference profile on the Roofline plane. MLA (blue dots) consistently achieves the highest operational intensity (*OI*) and attainable performance (*GFLOPS*) across all four sequence scenarios. By utilizing latent compression for the KV cache, MLA substantially reduces the volume of data movement required for each decoding step compared to the standard MHA, thereby shifting the execution significantly closer to the Roofline ridge point. Interestingly, at this specific 1.5B scale on edge hardware, GQA (red dots) exhibits the lowest efficiency among the three. It indicates that while GQA reduces the number of Key/Value heads, the latent-based compression in MLA provides a more effective balance between memory traffic reduction and computational throughput for on-device decoding.

Insight.4. *Attention architecture is a decisive factor for decoding efficiency: MLA outperforms both MHA and GQA by effectively compressing KV cache traffic to maximize operational intensity on resource-constrained devices.*

5. A Fairness-View: Hardware Utilization Efficiency

Hardware utilization efficiency is constrained by the intrinsic disparities of heterogeneous platforms and the structural

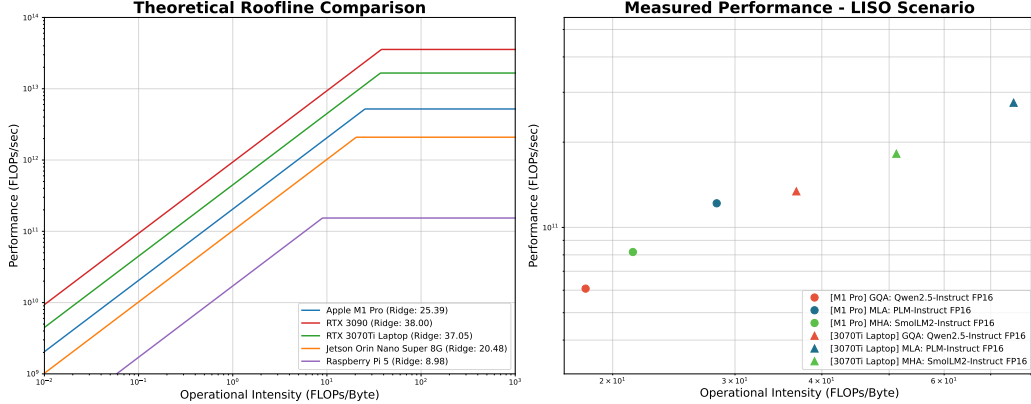


Figure 5. Analysis of hardware utilization efficiency and architectural scalability across heterogeneous platforms. The left panel presents the Theoretical Roofline Comparison for five representative devices including RTX 3090, RTX 3070Ti Laptop, Apple M1 Pro, Jetson Orin Nano, and Raspberry Pi 5, illustrating a significant disparity in theoretical ridge points ranging from 8.98 to 38.00 $FLOPs/Byte$. The right panel depicts the Measured Performance in the LISO scenario for MLA, MHA, and GQA configurations across the Apple M1 Pro and RTX 3070Ti Laptop, highlighting the consistent efficiency baseline and parallel shift in operational intensity and performance when scaling across hardware tiers.

variations of model architectures. This section evaluates the fairness of on-device inference by analyzing performance gaps across diverse hardware environments (Sec. 5.1) and examining how architectural choices influence the equity of resource saturation at a unified model scale (Sec. 5.2).

5.1. Disparity across Heterogeneous Hardware Platforms

Hardware utilization efficiency is strictly governed by the physical constraints of the underlying platform. As illustrated in Fig. 5, the theoretical Roofline profiles of five representative devices, ranging from the high-performance RTX 3090 to the ultra-low-power Raspberry Pi 5, reveal a staggering disparity in hardware capabilities. The theoretical peak performance spans three orders of magnitude from 10^{11} to 10^{13} FLOPs/sec, while the memory bandwidth defines distinct operational boundaries for each platform.

The critical indicator of hardware unfairness is the theoretical ridge point, which dictates the minimum OI required to saturate computational resources. High-performance GPUs such as the RTX 3090 (Ridge: 38.00) and RTX 3070Ti Laptop (Ridge: 37.05) possess significantly higher ridge points, meaning they require a much higher OI to transition from memory-bound to compute-bound regimes. In contrast, edge-side chips like the Apple M1 Pro (Ridge: 25.39), Jetson Orin Nano (Ridge: 20.48) and Raspberry Pi 5 (Ridge: 8.98) have much lower ridge points. While these devices are easier to saturate, their absolute performance ceilings are considerably lower. This disparity implies that a specific model architecture, such as a 1.5B model in the LISO scenario, may achieve near-optimal saturation on a Jetson Orin or Raspberry Pi but remain severely underutilized on an RTX 3090 because of the structural differences in theoretical memory-to-compute ratios.

Insight 5. *Hardware heterogeneity creates an "efficiency trap": the disparity in ridge points across devices ensures that a single model architecture cannot achieve uniform utilization equity, as the same operational intensity leads to vastly different bottleneck regimes on different platforms.*

5.2. Architectural Sensitivity of Utilization Equity

The cross-platform evaluation demonstrates that the efficiency dividends of architectural optimization are consistently preserved across varying hardware tiers. As illustrated in Fig. 6, we analyze the performance of different architectural configurations including MLA, MHA, and GQA on the Apple M1 Pro and the RTX 3070Ti Laptop under the compute-intensive LISO scenario. The results indicate that as the execution environment scales from an edge SoC to a high-performance GPU, all architectural designs benefit from increased memory bandwidth and computational peaks, resulting in a parallel shift toward the upper-right region of the Roofline plane.

Despite the collective performance gains, the relative hierarchy of utilization equity remains sensitive to the specific architectural design. MLA (blue markers) consistently maintains a superior position in both operational intensity (OI) and attainable performance ($GFLOPS$) on both platforms. Rather than being a platform-specific enhancement, the latent-based compression in MLA functions as a robust efficiency baseline. This stability proves that optimized architectural structures can reliably capture available hardware resources across the device spectrum, ensuring that the performance advantages of high-end accelerators are not overshadowed by the structural inefficiencies of traditional attention mechanisms.

Insight.6. Architectural optimization demonstrates consistent cross-platform robustness because while hardware scaling elevates the performance of all configurations, optimized structures such as MLA maintain a higher baseline of operational intensity and attainable performance, ensuring superior utilization of heterogeneous computational resources.

6. Discussion

Synergy between Architectural Innovation and Hardware Constraints The architectural evolution toward Multi head Latent Attention (MLA), as seen in DeepSeek V2(DeepSeek-AI, 2024) and PLM(Deng et al., 2025), along with the trainable sparse attention mechanism in MiniCPM(Hu et al., 2024), exemplifies the necessity of hardware aware innovation to transcend the memory wall in on device environments. MLA utilizes latent compression for the KV cache to reduce the volume of data movement required for each decoding step. Simultaneously, the sparse attention in MiniCPM reduces computational overhead by processing less than 5% of tokens in long context scenarios. Both structural choices elevate the operational intensity (OI) and shift the inference profile toward the compute bound regime. As shown in the cross platform comparison, MLA based configurations achieve a higher proficiency in capturing available computational peaks on high performance hardware compared to traditional mechanisms. Such synergy suggests that future on device architectures should prioritize optimizations such as latent compression or trainable sparsity to better align with the divergent theoretical ridge points of heterogeneous hardware.

Evolution of Capacity Density in Resource-Constrained Environments Capacity density, defined as the ratio of effective to actual parameter size, provides a unified framework for evaluating model quality according to the Densing Law(Xiao et al., 2024). This metric is crucial for resource-constrained environments where traditional scaling through model size is increasingly unsustainable. Layer-wise analysis of models such as Qwen2.5(Yang et al., 2024) reveals that operational intensity (OI) does not scale linearly with depth but reaches a peak at low layer counts. In the LISO scenario, increasing depth beyond this optimal threshold leads to an OI fallback. Because edge platforms such as the Raspberry Pi 5 or Jetson Orin Nano have low theoretical ridge points, they are highly sensitive to OI fluctuations. Consequently, improving the capacity density of shallow architectures is a more sustainable strategy for on-device intelligence than simply stacking layers, as it maximizes effective parameters within a restricted memory footprint.

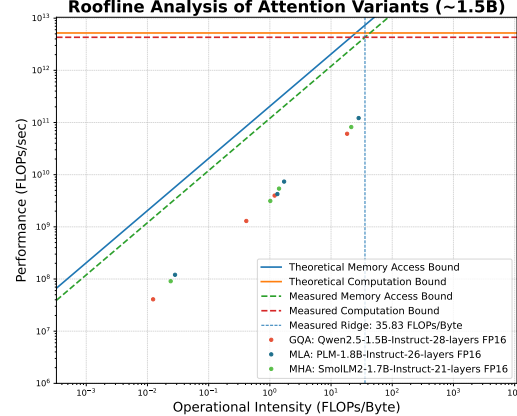


Figure 6. Impact of MHA, GQA, and MLA architectures on inference efficiency. All models are scaled to 1.5B parameters and tested at FP16 precision on an Apple M1 Pro. The distribution across the Roofline plane illustrates the efficiency gains of latent-based attention variations.

Paradigm of Hardware-Targeted Specialization for Architectural Primitives The gap between theoretical peaks and realized throughput suggests that framework design must prioritize data movement over raw compute capacity. Although $TFLOPS$ have grown rapidly, inference remains fundamentally limited by memory access patterns across diverse devices. Refining the interaction between hierarchical memory structures and execution kernels is essential to mitigate the bandwidth constraints that govern large scale model deployment. Additionally, hardware heterogeneity necessitates specializing AI compute units for specific high load primitives. General purpose logic frequently fails to exploit the structural advantages of modern architectures, leading to efficiency losses in on device scenarios. Hardware level optimization for critical primitives such as MLA and sparse attention is therefore crucial for maximizing throughput. Dedicated silicon support ensures that the theoretical operational intensity (OI) of optimized models can reach its full potential in real world execution.

7. Conclusion

We characterize LLM inference on edge devices using the Roofline model and introduce *Relative Inference Potential* to compare efficiency across heterogeneous substrates. Findings show that sequence length dictates distinct performance and operational intensity (OI) dynamics. We identify a non-monotonic OI trajectory: performance initially rises via overhead amortization but regresses beyond 3–5 layers as parameter loading outpaces computational reuse. Our analysis reveals an efficiency trap from hardware ridge-point disparities, while structural refinements sustain higher OI via optimized cache management. These results advocate for hardware-software co-design to align model architectures with physical constraints and unlock localized intelligence.

References

Abdin, M. I., Jacobs, S. A., Awan, A. A., Aneja, J., Awadallah, A., Awadalla, H., Bach, N., Bahree, A., Bakhtiari, A., Behl, H. S., Benhaim, A., Bilenko, M., Bjorck, J., Bubeck, S., Cai, M., Mendes, C. C. T., Chen, W., Chaudhary, V., Chopra, P., Giorno, A. D., de Rosa, G., Dixon, M., Eldan, R., Iter, D., Garg, A., Goswami, A., Gunasekar, S., Haider, E., Hao, J., Hewett, R. J., Huynh, J., Javaheripi, M., Jin, X., Kauffmann, P., Karampatziakis, N., Kim, D., Khademi, M., Kurilenko, L., Lee, J. R., Lee, Y. T., Li, Y., Liang, C., Liu, W., Lin, E., Lin, Z., Madan, P., Mitra, A., Modi, H., Nguyen, A., Norick, B., Patra, B., Perez-Becker, D., Portet, T., Pryzant, R., Qin, H., Radmilac, M., Rosset, C., Roy, S., Ruwase, O., Saarikivi, O., Saeid, A., Salim, A., Santacroce, M., Shah, S., Shang, N., Sharma, H., Song, X., Tanaka, M., Wang, X., Ward, R., Wang, G., Witte, P. A., Wyatt, M., Xu, C., Xu, J., Yadav, S., Yang, F., Yang, Z., Yu, D., Zhang, C., Zhang, C., Zhang, J., Zhang, L. L., Zhang, Y., Zhang, Y., Zhang, Y., and Zhou, X. Phi-3 technical report: A highly capable language model locally on your phone. *CoRR*, abs/2404.14219, 2024. doi: 10.48550/ARXIV.2404.14219. URL <https://doi.org/10.48550/arXiv.2404.14219>.

Agarwal, M., Qureshi, A., Sardana, N., Li, L., Quevedo, J., and Khudia, D. <https://www.databricks.com/blog/llm-inference-performance-engineering-best-practices>, 2023.

Alizadeh, K., Mirzadeh, I., Belenko, D., Khatamifard, S., Cho, M., del Mundo, C. C., Rastegari, M., and Farajtabar, M. LLM in a flash: Efficient large language model inference with limited memory. In Ku, L., Martins, A., and Srikumar, V. (eds.), *Proceedings of the 62nd Annual Meeting of the Association for Computational Linguistics (Volume 1: Long Papers)*, ACL 2024, Bangkok, Thailand, August 11-16, 2024, pp. 12562–12584. Association for Computational Linguistics, 2024. doi: 10.18653/V1/2024.ACL-LONG.678. URL <https://doi.org/10.18653/v1/2024.acl-long.678>.

Chen, L., Zaharia, M., and Zou, J. Frugalgpt: How to use large language models while reducing cost and improving performance. *Trans. Mach. Learn. Res.*, 2024, 2024. URL <https://openreview.net/forum?id=cSimKw5p6R>.

Chowdhery, A., Narang, S., Devlin, J., Bosma, M., Mishra, G., Roberts, A., Barham, P., Chung, H. W., Sutton, C., Gehrmann, S., Schuh, P., Shi, K., Tsvyashchenko, S., Maynez, J., Rao, A., Barnes, P., Tay, Y., Shazeer, N., Prabhakaran, V., Reif, E., Du, N., Hutchinson, B., Pope, R., Bradbury, J., Austin, J., Isard, M., Gur-Ari, G., Yin, P., Duke, T., Levskaya, A., Ghemawat, S., Dev, S., Michalewski, H., Garcia, X., Misra, V., Robinson, K., Fedus, L., Zhou, D., Ippolito, D., Luan, D., Lim, H., Zoph, B., Spiridonov, A., Sepassi, R., Dohan, D., Agrawal, S., Omernick, M., Dai, A. M., Pillai, T. S., Pelлат, M., Lewkowycz, A., Moreira, E., Child, R., Polozov, O., Lee, K., Zhou, Z., Wang, X., Saeta, B., Diaz, M., Firat, O., Catasta, M., Wei, J., Meier-Hellstern, K., Eck, D., Dean, J., Petrov, S., and Fiedel, N. PaLM: Scaling language modeling with pathways. *J. Mach. Learn. Res.*, 24:240:1–240:113, 2023.

Dao, T., Fu, D. Y., Ermon, S., Rudra, A., and Ré, C. Flashattention: Fast and memory-efficient exact attention with io-awareness, 2022. URL <https://arxiv.org/abs/2205.14135>.

DeepSeek-AI. Deepseek-v2: A strong, economical, and efficient mixture-of-experts language model. *CoRR*, abs/2405.04434, 2024. doi: 10.48550/ARXIV.2405.04434. URL <https://doi.org/10.48550/arXiv.2405.04434>.

Deng, C., Sun, L., Jiang, J., Zeng, Y., Wu, X., Zhao, W., Xiao, Q., Wang, J., Li, H., Chen, L., Ni, L. M., Zhang, H., and Wang, J. PLM: efficient peripheral language models hardware-co-designed for ubiquitous computing. *CoRR*, abs/2503.12167, 2025. doi: 10.48550/ARXIV.2503.12167. URL <https://doi.org/10.48550/arXiv.2503.12167>.

Frantar, E., Ashkboos, S., Hoefer, T., and Alistarh, D. GPTQ: accurate post-training quantization for generative pre-trained transformers. *CoRR*, abs/2210.17323, 2022. doi: 10.48550/ARXIV.2210.17323. URL <https://doi.org/10.48550/arXiv.2210.17323>.

Hendrycks, D., Burns, C., Basart, S., Zou, A., Mazeika, M., Song, D., and Steinhardt, J. Measuring massive multitask language understanding. In *9th International Conference on Learning Representations, ICLR 2021, Virtual Event, Austria, May 3-7, 2021*. OpenReview.net, 2021. URL <https://openreview.net/forum?id=d7KBjmI3GmQ>.

Hoffmann, J., Borgeaud, S., Mensch, A., Buchatskaya, E., Cai, T., Rutherford, E., de Las Casas, D., Hendricks, L. A., Welbl, J., Clark, A., Hennigan, T., Noland, E., Millican, K., van den Driessche, G., Damoc, B., Guy, A., Osindero, S., Simonyan, K., Elsen, E., Rae, J. W., Vinyals, O., and Sifre, L. Training compute-optimal large language models. *CoRR*, abs/2203.15556, 2022. doi: 10.48550/ARXIV.2203.15556. URL <https://doi.org/10.48550/arXiv.2203.15556>.

Hu, S., Tu, Y., Han, X., He, C., Cui, G., Long, X., Zheng, Z., Fang, Y., Huang, Y., Zhao, W., Zhang, X., Thai, Z. L., Zhang, K., Wang, C., Yao, Y., Zhao, C., Zhou, J., Cai, 9

J., Zhai, Z., Ding, N., Jia, C., Zeng, G., Li, D., Liu, Z., and Sun, M. Minicpm: Unveiling the potential of small language models with scalable training strategies. *CoRR*, abs/2404.06395, 2024. doi: 10.48550/ARXIV.2404.06395. URL <https://doi.org/10.48550/arXiv.2404.06395>.

Jiang, Y., Fu, Y., Huang, Y., Nie, P., Lu, Z., Xue, L., He, C., Sit, M.-K., Xue, J., Dong, L., Miao, Z., Du, D., Xu, T., Zou, K., Ponti, E., and Mai, L. Moe-cap: Benchmarking cost, accuracy and performance of sparse mixture-of-experts systems, 2025. URL <https://arxiv.org/abs/2412.07067>.

Kaplan, J., McCandlish, S., Henighan, T., Brown, T. B., Chess, B., Child, R., Gray, S., Radford, A., Wu, J., and Amodei, D. Scaling laws for neural language models. *CoRR*, abs/2001.08361, 2020. URL <https://arxiv.org/abs/2001.08361>.

Li, C., Wong, C., Zhang, S., Usuyama, N., Liu, H., Yang, J., Naumann, T., Poon, H., and Gao, J. Llava-med: Training a large language-and-vision assistant for biomedicine in one day. In Oh, A., Naumann, T., Globerson, A., Saenko, K., Hardt, M., and Levine, S. (eds.), *Advances in Neural Information Processing Systems 36: Annual Conference on Neural Information Processing Systems 2023, NeurIPS 2023, New Orleans, LA, USA, December 10 - 16, 2023*, 2023. URL http://papers.nips.cc/paper_files/paper/2023/hash/5abcdf8ecdacba028c6662789194572-Abstract-Datasets_and_Benchmarks.html.

Liang, P., Bommasani, R., Lee, T., Tsipras, D., Soylu, D., Yasunaga, M., Zhang, Y., Narayanan, D., Wu, Y., Kumar, A., Newman, B., Yuan, B., Yan, B., Zhang, C., Cosgrove, C., Manning, C. D., Ré, C., Acosta-Navas, D., Hudson, D. A., Zelikman, E., Durmus, E., Ladhak, F., Rong, F., Ren, H., Yao, H., Wang, J., Santhanam, K., Orr, L. J., Zheng, L., Yüksekgönül, M., Suzgun, M., Kim, N., Guha, N., Chatterji, N. S., Khattab, O., Henderson, P., Huang, Q., Chi, R., Xie, S. M., Santurkar, S., Ganguli, S., Hashimoto, T., Icard, T., Zhang, T., Chaudhary, V., Wang, W., Li, X., Mai, Y., Zhang, Y., and Koreeda, Y. Holistic evaluation of language models. *Trans. Mach. Learn. Res.*, 2023, 2023. URL <https://openreview.net/forum?id=i04LZibEqW>.

Lin, J., Tang, J., Tang, H., Yang, S., Chen, W., Wang, W., Xiao, G., Dang, X., Gan, C., and Han, S. AWQ: activation-aware weight quantization for on-device LLM compression and acceleration. In Gibbons, P. B., Pekhimenko, G., and Sa, C. D. (eds.), *Proceedings of the Seventh Annual Conference on Machine Learning and Systems, MLSys 2024, Santa Clara, CA, USA, May 13-16, 2024*. mlsys.org, 2024. URL https://proceeding.s.mlsys.org/paper_files/paper/2024/hash/42a452cbafa9dd64e9ba4aa95cclef21-Abstract-Conference.html.

Liu, Z., Zhao, C., Iandola, F. N., Lai, C., Tian, Y., Fedorov, I., Xiong, Y., Chang, E., Shi, Y., Krishnamoorthi, R., Lai, L., and Chandra, V. Mobilellm: Optimizing sub-billion parameter language models for on-device use cases. In *Forty-first International Conference on Machine Learning, ICML 2024, Vienna, Austria, July 21-27, 2024*, 2024. URL <https://openreview.net/forum?id=EIGbXbxcUQ>.

Pope, R., Douglas, S., Chowdhery, A., Devlin, J., Bradbury, J., Heek, J., Xiao, K., Agrawal, S., and Dean, J. Efficiently scaling transformer inference. In Song, D., Carbin, M., and Chen, T. (eds.), *Proceedings of the Sixth Conference on Machine Learning and Systems, MLSys 2023, Miami, FL, USA, June 4-8, 2023*. mlsys.org, 2023. URL https://proceedings.mlsys.org/paper_files/paper/2023/hash/c4be71ab8d24cdfb45e3d06dbfca2780-Abstract-mlsys2023.html.

Prieto, P. and Abad, P. Edge deployment of small language models, a comprehensive comparison of cpu, GPU and NPU backends. *CoRR*, abs/2511.22334, 2025. doi: 10.48550/ARXIV.2511.22334. URL <https://doi.org/10.48550/arXiv.2511.22334>.

Rajesh, V., Jodhpurkar, O., Anbuselvan, P., Singh, M., Jallepali, A., Godbole, S., Sharma, P. K., and Shrivastava, H. Production-grade local LLM inference on apple silicon: A comparative study of mlx, mlc-llm, ollama, llama.cpp, and pytorch MPS. *CoRR*, abs/2511.05502, 2025. doi: 10.48550/ARXIV.2511.05502. URL <https://doi.org/10.48550/arXiv.2511.05502>.

Reddi, V. J., Cheng, C., Kanter, D., Mattson, P., Schmuelling, G., Wu, C., Anderson, B., Breughe, M., Charlebois, M., Chou, W., Chukka, R., Coleman, C., Davis, S., Deng, P., Diamos, G., Duke, J., Fick, D., Gardner, J. S., Hubara, I., Idgunji, S., Jablin, T. B., Jiao, J., John, T. S., Kanwar, P., Lee, D., Liao, J., Lokhmotov, A., Massa, F., Meng, P., Micikevicius, P., Osborne, C., Pekhimenko, G., Rajan, A. T. R., Sequeira, D., Sirasao, A., Sun, F., Tang, H., Thomson, M., Wei, F., Wu, E., Xu, L., Yamada, K., Yu, B., Yuan, G., Zhong, A., Zhang, P., and Zhou, Y. Mlperf inference benchmark. *CoRR*, abs/1911.02549, 2019. URL <http://arxiv.org/abs/1911.02549>.

Sun, L., Jiang, J., Deng, C., Wu, X., Zhang, H., Chen, L., Ni, L. M., and Wang, J. GTA: grouped-head latent attention. *CoRR*, abs/2506.17286, 2025. doi: 10.48550/ARXIV.2506.17286. URL <https://doi.org/10.48550/arXiv.2506.17286>.

Team, G. Gemma: Open models based on gemini research and technology. *CoRR*, abs/2403.08295, 2024a. doi: 10.48550/ARXIV.2403.08295. URL <https://doi.org/10.48550/arXiv.2403.08295>.

Team, L. The llama 3 herd of models. *CoRR*, abs/2407.21783, 2024b. doi: 10.48550/ARXIV.2407.21783. URL <https://doi.org/10.48550/arXiv.2407.21783>.

Touvron, H., Martin, L., Stone, K., Albert, P., Almahairi, A., Babaei, Y., Bashlykov, N., Batra, S., Bhargava, P., Bhosale, S., Bikel, D., Blecher, L., Canton-Ferrer, C., Chen, M., Cucurull, G., Esiobu, D., Fernandes, J., Fu, J., Fu, W., Fuller, B., Gao, C., Goswami, V., Goyal, N., Hartshorn, A., Hosseini, S., Hou, R., Inan, H., Kardas, M., Kerkez, V., Khabsa, M., Kloumann, I., Korenev, A., Koura, P. S., Lachaux, M., Lavril, T., Lee, J., Liskovich, D., Lu, Y., Mao, Y., Martinet, X., Mihaylov, T., Mishra, P., Molybog, I., Nie, Y., Poulton, A., Reizenstein, J., Rungta, R., Saladi, K., Schelten, A., Silva, R., Smith, E. M., Subramanian, R., Tan, X. E., Tang, B., Taylor, R., Williams, A., Kuan, J. X., Xu, P., Yan, Z., Zarov, I., Zhang, Y., Fan, A., Kambadur, M., Narang, S., Rodriguez, A., Stojnic, R., Edunov, S., and Scialom, T. Llama 2: Open foundation and fine-tuned chat models. *CoRR*, abs/2307.09288, 2023. doi: 10.48550/ARXIV.2307.09288. URL <https://doi.org/10.48550/arXiv.2307.09288>.

Williams, S., Waterman, A., and Patterson, D. A. Roofline: an insightful visual performance model for multicore architectures. *Commun. ACM*, 52(4):65–76, 2009. doi: 10.1145/1498765.1498785. URL <https://doi.org/10.1145/1498765.1498785>.

Xiao, C., Cai, J., Zhao, W., Zeng, G., Lin, B., Zhou, J., Zheng, Z., Han, X., Liu, Z., and Sun, M. Densing law of llms. *CoRR*, abs/2412.04315, 2024. doi: 10.48550/ARXIV.2412.04315. URL <https://doi.org/10.48550/arXiv.2412.04315>.

Yang, A., Yang, B., Zhang, B., Hui, B., Zheng, B., Yu, B., Li, C., Liu, D., Huang, F., Wei, H., Lin, H., Yang, J., Tu, J., Zhang, J., Yang, J., Yang, J., Zhou, J., Lin, J., Dang, K., Lu, K., Bao, K., Yang, K., Yu, L., Li, M., Xue, M., Zhang, P., Zhu, Q., Men, R., Lin, R., Li, T., Xia, T., Ren, X., Ren, X., Fan, Y., Su, Y., Zhang, Y., Wan, Y., Liu, Y., Cui, Z., Zhang, Z., and Qiu, Z. Qwen2.5 technical report. *CoRR*, abs/2412.15115, 2024. doi: 10.48550/ARXIV.2412.15115. URL <https://doi.org/10.48550/arXiv.2412.15115>.

Yao, Y., Yu, T., Zhang, A., Wang, C., Cui, J., Zhu, H., Cai, T., Li, H., Zhao, W., He, Z., Chen, Q., Zhou, H., Zou, Z., Zhang, H., Hu, S., Zheng, Z., Zhou, J., Cai, J., Han, X., Zeng, G., Li, D., Liu, Z., and Sun, M. Minicpm-v: A GPT-4V level MLLM on your phone. *CoRR*, abs/2408.01800, 2024. doi: 10.48550/ARXIV.2408.01800. URL <https://doi.org/10.48550/arXiv.2408.01800>.

Yu, T., Wang, Z., Wang, C., Huang, F., Ma, W., He, Z., Cai, T., Chen, W., Huang, Y., Zhao, Y., Xu, B., Cui, J., Xu, Y., Ruan, L., Zhang, L., Liu, H., Tang, J., Liu, H., Guo, Q., Hu, W., He, B., Zhou, J., Cai, J., Qi, J., Guo, Z., Chen, C., Zeng, G., Li, Y., Cui, G., Ding, N., Han, X., Yao, Y., Liu, Z., and Sun, M. Minicpm-v 4.5: Cooking efficient mllms via architecture, data, and training recipe, 2025. URL <https://arxiv.org/abs/2509.18154>.

Zhang, P., Zeng, G., Wang, T., and Lu, W. Tinylama: An open-source small language model. *CoRR*, abs/2401.02385, 2024. doi: 10.48550/ARXIV.2401.02385. URL <https://doi.org/10.48550/arXiv.2401.02385>.

Zheng, Y., Chen, Y., Qian, B., Shi, X., Shu, Y., and Chen, J. A review on edge large language models: Design, execution, and applications. *ACM Comput. Surv.*, 57(8):209:1–209:35, 2025. doi: 10.1145/3719664. URL <https://doi.org/10.1145/3719664>.

A. Related Work

Trends in Efficient LLMs. With the rapid proliferation of open-source foundation models such as the Llama series (Touvron et al., 2023) (Team, 2024b), scaling laws (Kaplan et al., 2020) have revealed a positive correlation between model capability and parameter scale, driving the trend toward increasingly massive models. However, driven by concerns regarding data privacy, latency sensitivity, and operational costs, deploying LLMs on on-device hardware has become an imperative, catalyzing a fundamental paradigm shift from cloud-based inference to edge computing (Zheng et al., 2025). To accommodate constrained on-device resources, compact architectures optimized for mobile scenarios have emerged, such as TinyLlama (Zhang et al., 2024) and MobileLLM (Liu et al., 2024). Concurrently, mature post-training quantization techniques like GPTQ (Frantar et al., 2022) and AWQ (Lin et al., 2024) have significantly reduced memory footprints and computational loads. Despite these advancements in model compression, as noted by Alizadeh et al. (Alizadeh et al., 2024), the performance bottleneck for generative LLMs on edge devices is typically strictly governed by memory bandwidth rather than compute capacity (the "Memory Wall"). The limitations of these hardware characteristics necessitate a more profound, hardware-aware analysis of inference performance, moving beyond a mere evaluation of inference metrics.

General Capabilities Benchmarking. Existing evaluation frameworks for Large Language Models (LLMs) predominantly focus on their cognitive and linguistic capabilities. Among these, MMLU (Hendrycks et al., 2021) serves as a foundational benchmark, covering 57 tasks across diverse domains such as mathematics, history, and law to assess multi-task problem-solving abilities. Furthermore, HELM (Liang et al., 2023) implements a holistic, multi-metric approach to evaluate dozens of mainstream LLMs, offering a comprehensive view of their semantic performance across various core scenarios.

While these benchmarks are essential for measuring "model intelligence," they typically treat the inference process as a system-agnostic black box. Consequently, they prioritize task-specific accuracy while disregarding the underlying computational overhead, such as system efficiency, real-time resource consumption, and hardware utilization. For resource-constrained edge devices, relying solely on these capability-centric metrics is insufficient to guarantee deployment viability, underscoring the urgent need for a more granular, system-level evaluation perspective.

System Efficiency and On-Device Benchmarking. To bridge the gap between algorithmic capability and physical deployment, recent research has shifted toward system-level efficiency. Industry standards like MLPerf (Reddi et al., 2019) establish rigorous protocols for evaluating inference systems across heterogeneous backends, while FrugalGPT (Chen et al., 2024) introduces a cost-centric perspective, analyzing the trade-offs between API expenditures and model performance.

Specifically for on-device environments, several recent studies have provided in-depth empirical analyses. Edge Deployment of SLMs (Prieto & Abad, 2025) conducts a comprehensive evaluation across mobile CPUs, GPUs, and NPUs, highlighting the superior energy efficiency of NPUs and the necessity of bandwidth normalization for cross-architecture fairness. Within specific hardware ecosystems, Local LLM Inference on Apple Silicon (Rajesh et al., 2025) systematically compares runtimes such as MLX and MLC-LLM, characterizing their throughput and latency within unified memory architectures. Furthermore, for sparse models, MoE-CAP (Jiang et al., 2025) identifies the inherent trade-offs between Cost, Accuracy, and Performance (CAP), proposing sparsity-aware utilization metrics.

Despite these advancements, a fundamental limitation persists: existing benchmarks primarily report observed execution metrics (e.g., TTFT, throughput) without contextualizing them against the theoretical limits of the hardware. Such empirical observations often fail to decouple software-level optimizations from inherent hardware capabilities, potentially leading to biased conclusions regarding architectural efficiency. Our work addresses this gap by leveraging the Roofline Model (Williams et al., 2009). By characterizing performance as a function of arithmetic intensity and hardware ceilings (peak compute and memory bandwidth), our framework enables a more transparent and fair benchmarking process that quantifies how effectively an LLM implementation approaches its hardware's theoretical potential.

B. Future Work

While this study provides an extensive empirical characterization of mainstream small language models across diverse hardware tiers, we identify several strategic avenues for future exploration. Primarily, we intend to expand the taxonomy of our benchmarking framework to incorporate a broader range of attention mechanisms. Although our current analysis provides a comprehensive evaluation of critical patterns such as *MLA* and *GQA*, we aim to adapt our methodology to emerging structural variants and hybrid architectures to ensure the continued relevance of our operational intensity (*OI*) insights across the evolving architectural landscape.

A significant frontier lies in the analytical characterization of Mixture of Experts (MoE) architectures. Quantifying the theoretical *FLOPS* for MoE models during dynamic inference remains a formidable challenge because the stochastic nature of token routing complicates the estimation of the execution ceiling. While the current work focuses on dense architectures, extending the Roofline model to account for sparse activation regimes will be essential for identifying the unique physical constraints and efficiency traps inherent in localized MoE deployment.

Finally, we plan to broaden the experimental scope across both hardware and software dimensions. On the hardware side, we aim to scale our testing to a more diverse array of heterogeneous edge devices to further validate the cross platform robustness of our findings. On the software side, we recognize that different inference engines, such as TensorRT LLM, vLLM, and ONNX Runtime, introduce substantial variance in performance. Investigating how these software stacks influence *OI* and realized throughput will provide a more holistic understanding of the entire deployment pipeline, facilitating a more effective transition toward true hardware software co design.

C. Experimental Details

The code for this work is available at https://github.com/banbu-ai/roofline_bench.

C.1. Evaluated Model Architectures

To investigate the scaling laws and efficiency of intelligence on-device, we select a diverse set of models that represent current trends in localized AI. These models are evaluated across two categories based on the computational tiers of the hardware substrates:

- **Edge-Scale Models:** For the most resource-limited tier represented by the Raspberry Pi 5, we evaluate ultra-compact models including the Pythia (160M, 410M), Qwen2.5-0.5B, and SmolLM2 (135M, 360M) families. These models primarily utilize Q8_0 quantization to fit within the constraints of general-purpose CPUs.
- **Mobile-Class Models:** For performance-oriented platforms such as the Apple M1 Pro, RTX 3070 Ti Laptop, and Jetson Orin Nano Super, we employ models ranging from 0.6B to 1.8B parameters. This group features diverse types of attention to observe their impact on the potential for inference, including Grouped-Query Attention (GQA) for Qwen2.5-1.5B, Llama-3.2-1B, Qwen3-0.6B, and Fox-1-1.6B; Multi-Head Attention (MHA) for SmolLM2-1.7B; and Multi-Head Latent Attention (MLA) for PLM-1.8B.

All architectures are tested under four distinct scenarios—SISO, LISO, SILO, and LILO—to capture performance dynamics across varying sequence lengths. This selection provides a rigorous basis for the co-design of models and hardware by identifying how structural primitives like attention mechanisms interact with physical memory boundaries.

C.2. Evaluated Hardware Substrates

To ensure a rigorous evaluation across various tiers of computation, we conduct our analysis on four distinct hardware platforms. These substrates represent a broad spectrum of architectural designs and power envelopes, reflecting the diverse physical constraints encountered in on-device intelligence. The selection includes the Apple M1 Pro (a unified system on a chip), the RTX 3070 Ti Laptop (a discrete GPU for mobile workstations), the Jetson Orin Nano Super (a dedicated module for AI at the edge), and the Raspberry Pi 5 (a ubiquitous platform based on a general CPU).

Table 1 summarizes the specifications for heterogeneous platforms, ranging from Discrete GPUs to General CPUs. By incorporating theoretical and measured values for peak performance (π) and memory bandwidth (β), these metrics establish the boundaries for calculating Relative Inference Potential (Φ). Such characterization is essential to identify requirements for effective hardware-software co-design in intelligence on-device.

C.3. Experimental Setting

Hardware Characterization and Roofline Benchmarking. To establish the empirical bounds for the Roofline model, we evaluate the peak throughput and memory bandwidth across a heterogeneous suite of devices, including macOS, Windows, NVIDIA Jetson Orin Nano, and Raspberry Pi platforms. We conduct synthetic benchmarks involving large-scale matrix addition and multiplication using the PyTorch framework. To ensure optimal performance across architectures, we utilize

Table 1. Hardware Specifications and Performance Metrics across Heterogeneous Platforms. Theo denotes the theoretical peak value provided by the manufacturer, while Meas denotes the measured peak performance under benchmarking workloads. Notably, the measured FP16 peak performance for NVIDIA RTX 30 series GPUs and Jetson Orin Nano significantly exceeds their theoretical FP32 peak values because of the activation of specialized hardware such as Tensor Cores during evaluation. Values marked with \dagger are in GFLOPS, while all other compute metrics are in TFLOPS.

Chip	Architecture	Bandwidth (GB/s) Theo / Meas	FP16 Peak (TFLOPS) Theo / Meas	FP32 Peak (TFLOPS) Theo / Meas
NVIDIA RTX 3090	Discrete GPU	936.20 / 560.02	35.58 / 66.20	35.58 / 24.28
NVIDIA RTX 3070 Ti Laptop	Discrete GPU	448.00 / 217.00	16.60 / 31.76	16.60 / 9.51
Apple M1 Pro	Unified SoC	204.80 / 120.03	— / 4.61	5.20 / 4.31
Jetson Orin Nano Super 8G	Edge AI Module	102.00 / 59.40	4.178 / 9.56	2.089 / 1.34
Raspberry Pi 5	General CPU	17.10 / 3.98	— / 1.48 \dagger	153.60 \dagger / 78.56 \dagger

the CUDA backend for NVIDIA hardware and the Metal Performance Shaders (MPS) backend for Apple Silicon devices. These measurements provide the hardware-specific constants required for our performance analysis.

FLOPs Calculation Methodology. To evaluate operational intensity (OI) and performance within the Roofline model, we estimate the floating point operations (*FLOPs*) associated with each inference configuration. This estimation framework accounts for linear projections, attention mechanisms, and KV cache management by leveraging key architectural parameters including the hidden dimension (h), the number of query heads (n_h), and the number of key-value heads (n_{kv}). The specific estimation logic [Sun et al. \(2025\)](#), with detailed formulas provided in Table 2. The resulting *FLOPs* values serve as an approximated baseline for deriving OI and throughput metrics.

Table 2. Comparison of computational complexity and memory requirements for different attention mechanisms. H is the hidden dimension, N is the sequence length, n_q, n_k, n_v, n_c are the number of query, key, value, and latent value heads, respectively; d_h is the per-head dimension, d_l is the latent dimension. For MLA-based structures, d_c denotes the KV compression dimension, while d_{rope} and d_{nope} represent the rotary and non-rotary components of the embedding dimension, respectively.

Attention	KV Cache per Layer	Attention	Computation per Layer		Expressivity
			Linear		
MHA	$2n_h d_h N$	$2n_h d_h N^2$	$4NH^2$		Strong
GQA	$2n_k d_h N$	$2n_h d_h N^2$	$2NH^2 + 2n_k d_h NH$		Moderate
MLA	$(d_c + d_{rope})N$	$n_h(d_{rope} + 2d_{nope})N^2$	$\left((d_c + d_{rope})H + n_h(d_{rope} + d_{nope})H + 2n_h d_l d_{nope} + H^2\right)N$		Strong
GVA	$(H + n_k d_h)N$	$(n_q d_h + n_h d_h)N^2$	$2NH^2 + 2n_k d_h NH$		Moderate
GHA	$(n_k d_h + n_v d_h)N$	$(n_q d_h + n_h d_h)N^2$	$NH^2 + n_q d_h NH + n_k d_h NH + n_v d_h NH$		Weak
GTA	$(n_k d_h + n_c d_l)N$	$n_q(d_k + d_l)N^2$	$2NH^2 + (n_q d_h + n_k d_h + n_c d_l + d_l)NH$		Strong

Inference Memory Monitoring. We employ platform-specific strategies to monitor memory utilization during llama-bench execution. For devices with Unified Memory Architectures (UMA)—including macOS and NVIDIA Jetson—as well as CPU-based platforms like the Raspberry Pi 5, we track physical memory usage by mapping the target process name to its Process ID (PID) and sampling its resident set size (RSS) during inference. On Windows systems equipped with consumer-grade discrete GPUs, monitoring process-specific VRAM presents a technical challenge. Due to the Windows Display Driver Model (WDDM) constraints on consumer hardware—which lack support for the Tesla Compute Cluster (TCC) mode required for granular per-process accounting—standard utilities such as nvidia-smi and pynvml often return null values for individual process memory. To circumvent this, we implement an exclusive-access monitoring strategy: by parsing nvidia-smi XML outputs, we ensure the discrete GPU is dedicated solely to the target PID during benchmarking. Under these isolated conditions, the total VRAM utilization of the device serves as a precise proxy for the inference memory footprint.

Inference Workflow and Data Acquisition. For each experimental trial, we execute llama-bench with parameterized input/output sequence lengths and thread counts. To ensure temporal synchronization across data streams, each session is assigned a unique timestamp. During execution, our framework concurrently monitors the memory footprint and records the runtime metrics. The resulting inference logs, formatted in JSON as per llama-bench specifications, capture comprehensive metadata including device architecture, backend configurations, model types, and specific command-line arguments. Upon completion of each inference cycle, our framework performs automated post-hoc analysis and computational evaluation

based on these synchronized logs and memory traces.

Memory Management and Offloading Strategy. While the inference framework allows for explicit control over offloading, we incorporate this strategy to handle scenarios where model depth exceeds the 8 GB VRAM capacity of the RTX 3070Ti Laptop. The observed linear performance degradation in specific experimental trials is primarily attributed to the automated offloading mechanism in llama.cpp. When the GPU-resident buffers are insufficient to accommodate weight tensors, the framework dynamically reallocates storage to system memory. This allocation follows a tiered priority hierarchy: ACCEL (accelerated CPU regions) → GPU Host (pinned memory for optimized DMA transfer) → CPU Extra → Standard CPU (general-purpose system memory).

D. Comprehensive Benchmarking Analysis of Model Architectures on Heterogeneous Hardware Platforms

This appendix provides a comprehensive suite of benchmarking results to substantiate the empirical findings and theoretical analyses presented in the main text. We detail the performance profiles of various large language model architectures including Multi head Latent Attention and trainable sparse attention across a spectrum of heterogeneous hardware platforms ranging from high performance accelerators to edge side SoCs. The presented data encompass a wide array of quantization precisions and operational scenarios while offering granular insights into the relationship between architectural design, layer wise operational intensity (OI), and hardware resource saturation. By providing these extended datasets, we aim to offer a rigorous validation of the scaling dynamics and utilization equity discussed throughout the study.

D.1. Analysis and Findings on the Optimality Gap

The vertical distance between the actual operating point and the theoretical Roofline ceiling in the performance chart (as illustrated across different devices in Figure 7). This gap quantifies the "left-on-the-table" performance and serves as a direct indicator of optimization headroom.

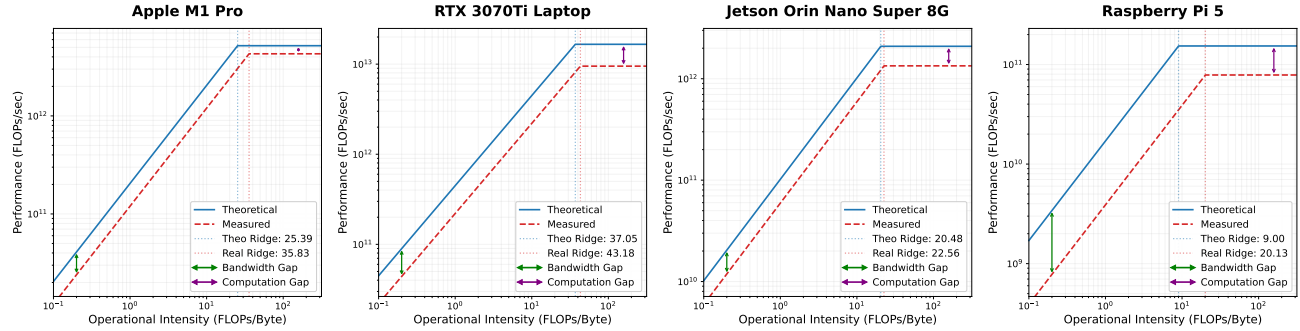


Figure 7. Performance gap analysis using Roofline models on different hardware. Green and purple arrows represent Bandwidth and Compute Gaps between theoretical (solid blue) and measured (dashed red) performance. Vertical lines mark the theoretical and real-world ridge points.

D.2. Extended Benchmark Results: Prefilling and Decoding TPS

Table 3. Detailed inference throughput (TPS) on Raspberry Pi 5 across various scenarios. Data are presented as Prefilling TPS / Decoding TPS.

Model	Precision	SISO	LISO	SILO	LILO
pythia-160m	Q8_0	149 / 70	63 / 71	150 / 25	64 / 27
pythia-410m	Q8_0	43 / 26	20 / 26	43 / 9	21 / 9
Qwen2.5-0.5B-Instruct	Q8_0	38 / 20	22 / 20	38 / 14	22 / 14
SmILM2-135M-Instruct	Q8_0	115 / 65	42 / 65	115 / 29	42 / 29
SmILM2-360M-Instruct	Q8_0	41 / 26	20 / 26	42 / 14	20 / 14

Table 4. Cross device inference throughput (TPS) comparison for Qwen2.5-1.5B-Instruct in Q8.0 precision. Data are presented as Prefilling TPS / Decoding TPS.

Model	Precision	Device	SISO	LISO	SILO	LILO
Qwen2.5-1.5B-Instruct	Q8.0	M1Pro	1349 / 63	1204 / 62	1349 / 52	1204 / 52
		RTX 3070Ti L	4465 / 127	5286 / 130	4295 / 118	5256 / 119
		Jetson Orin	1203 / 25	1075 / 25	1281 / 23	1073 / 23

Table 5. Detailed inference throughput (TPS) on Apple M1 Pro across various scenarios. Data are presented as Prefilling TPS / Decoding TPS.

Model	Precision	SISO	LISO	SILO	LILO
Qwen2.5-1.5B-Instruct	FP16	1424 / 50	1273 / 50	1423 / 43	1273 / 43
	Q8.0	1349 / 63	1204 / 62	1349 / 52	1204 / 52
	Q4_K_M	1199 / 90	1078 / 90	1200 / 69	1078 / 69
Qwen3-0.6B	FP16	3168 / 102	2140 / 102	3164 / 69	2143 / 71
	Q8.0	2984 / 105	2072 / 105	3018 / 72	2070 / 72
	Q4_K_M	2765 / 100	1939 / 160	2770 / 94	1942 / 94
Llama-3.2-1B-Instruct	FP16	2002 / 65	1594 / 65	2000 / 51	1594 / 51
	Q8.0	1894 / 92	1509 / 92	1894 / 67	1509 / 67
	Q4_K_M	1691 / 133	1369 / 133	1691 / 86	1370 / 85
PLM-1.8B-Instruct	FP16	1114 / 40	939 / 40	1113 / 30	939 / 30
	Q8.0	1053 / 55	891 / 55	1053 / 38	890 / 38
	Q4_K_M	942 / 75	812 / 75	942 / 46	812 / 46
Fox-1-1.6B	FP16	1522 / 47	1239 / 47	1521 / 38	1239 / 38
	Q8.0	1438 / 63	1174 / 63	1438 / 49	1174 / 49
	Q4_K_M	1295 / 87	1070 / 88	1295 / 62	1071 / 62
SmolLM2-1.7B-Instruct	FP16	1212 / 46	970 / 46	1212 / 35	971 / 35
	Q8.0	1139 / 64	918 / 64	1138 / 46	916 / 46
	Q4_K_M	1002 / 90	827 / 90	1002 / 58	827 / 58

D.3. Extended Empirical Characterization: Comprehensive Roofline Profiles

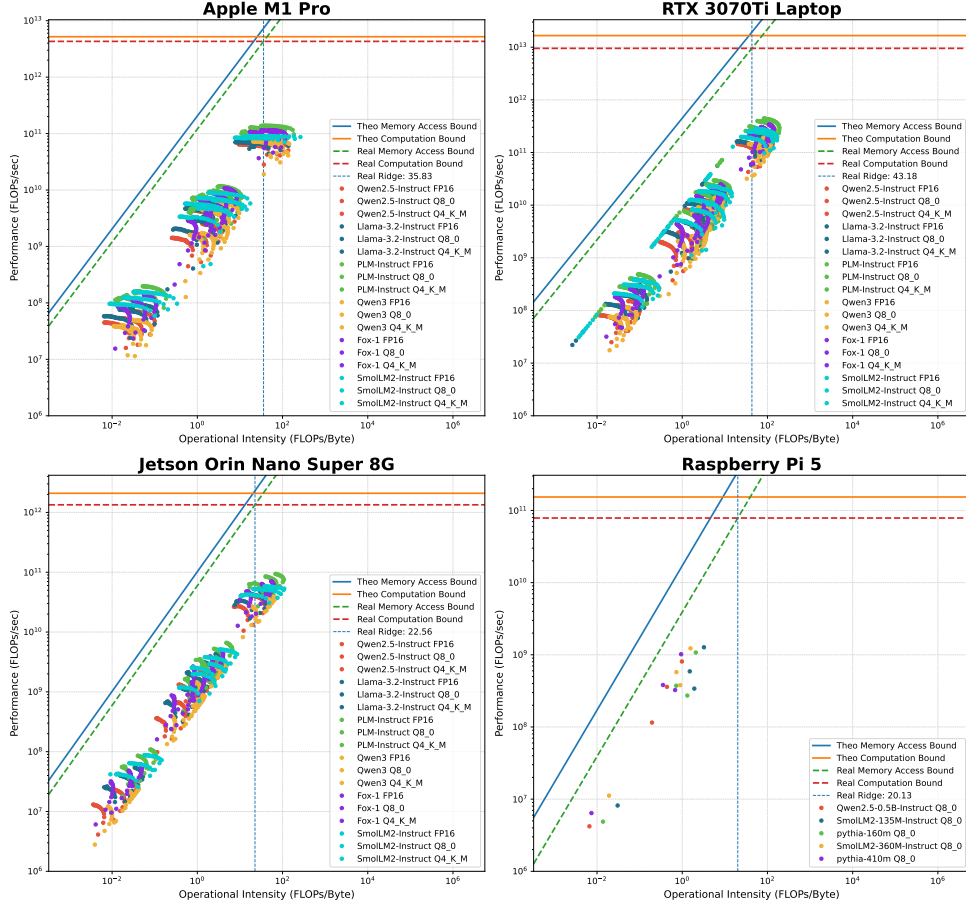


Figure 8. Hardware Specifications and Performance Metrics across Heterogeneous Platforms. Theo denotes the theoretical peak value provided by the manufacturer, while Meas denotes the measured peak performance under benchmarking workloads. Notably, the measured FP16 peak performance for NVIDIA RTX 30 series GPUs and Jetson Orin Nano significantly exceeds their theoretical FP32 peak values because of the activation of specialized hardware such as Tensor Cores during evaluation. Values marked with \dagger are in GFLOPS, while all other compute metrics are in TFLOPS.

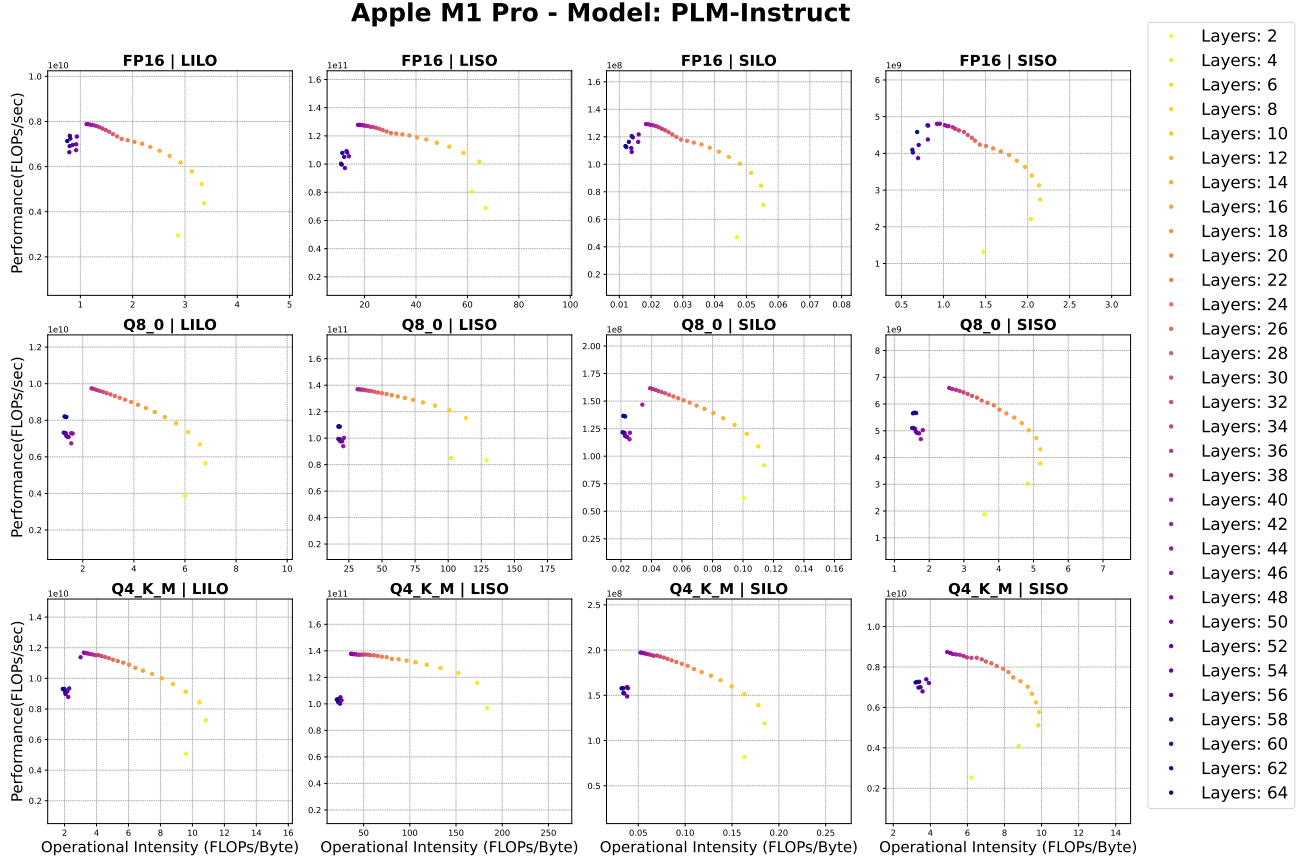


Figure 9. Layer-wise operational intensity trends for PLM-Instruct on Apple M1 Pro. This evaluation monitors the progression of computational intensity throughout the layer stack under diverse inference workloads. The profiles reveal that while most layers maintain a stable intensity, certain points exhibit a steep drop in metrics. Such abrupt decreases indicate that the model has reached a performance bottleneck, where the throughput is increasingly restricted by the underlying hardware architecture, leading to a noticeable reduction in layer-wise efficiency.

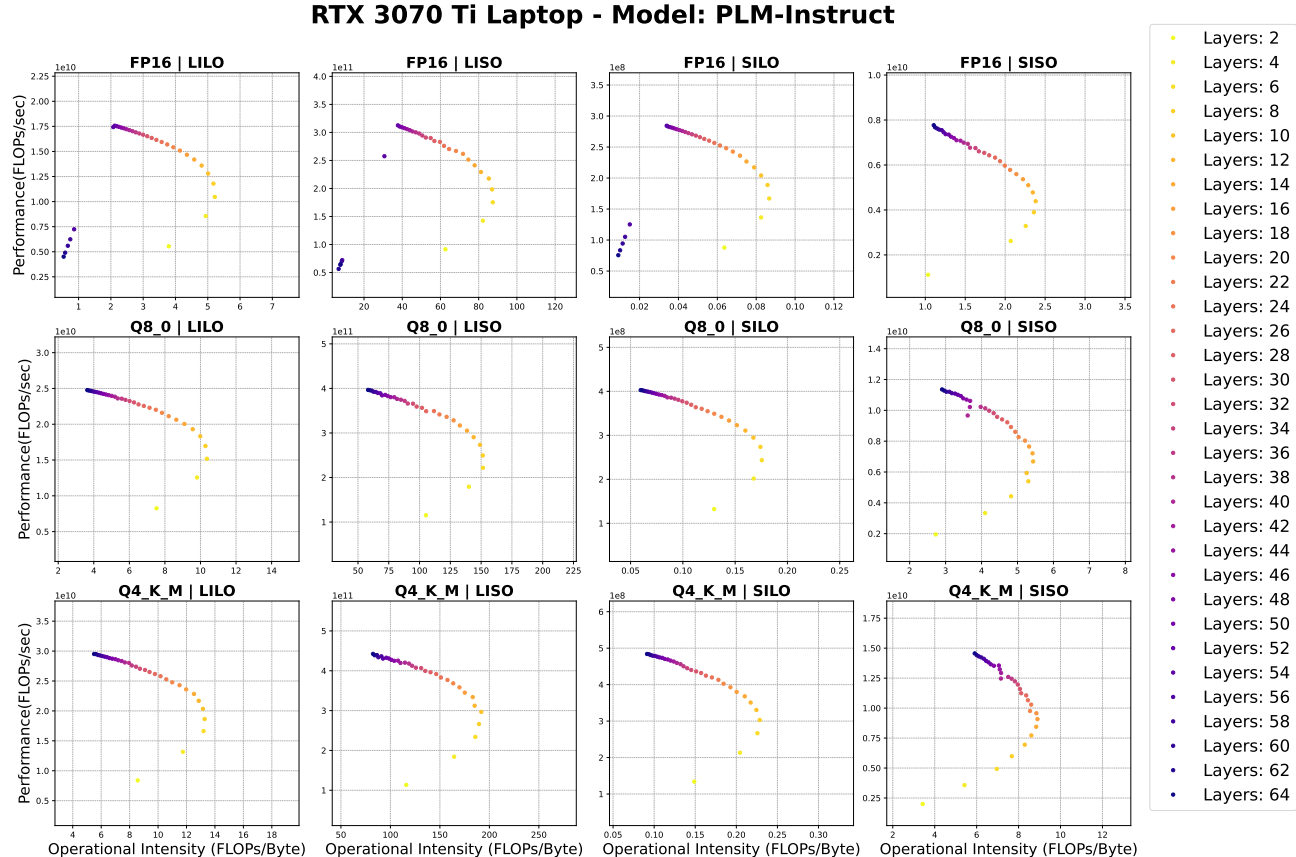


Figure 10. Layer-wise operational intensity trends for PLM-Instruct on NVIDIA RTX 3070 Ti Laptop. The subplots map the operational intensity (FLOPs/Byte) against the Transformer layer index across diverse inference workloads. Although the computational intensity is generally uniform throughout the layer stack, certain data points exhibit a significant downward trend. Such abrupt decreases mark the onset of hardware-specific bottlenecks, where the data movement or processing constraints lead to a noticeable reduction in layer-wise efficiency compared to the stable segments of the model.

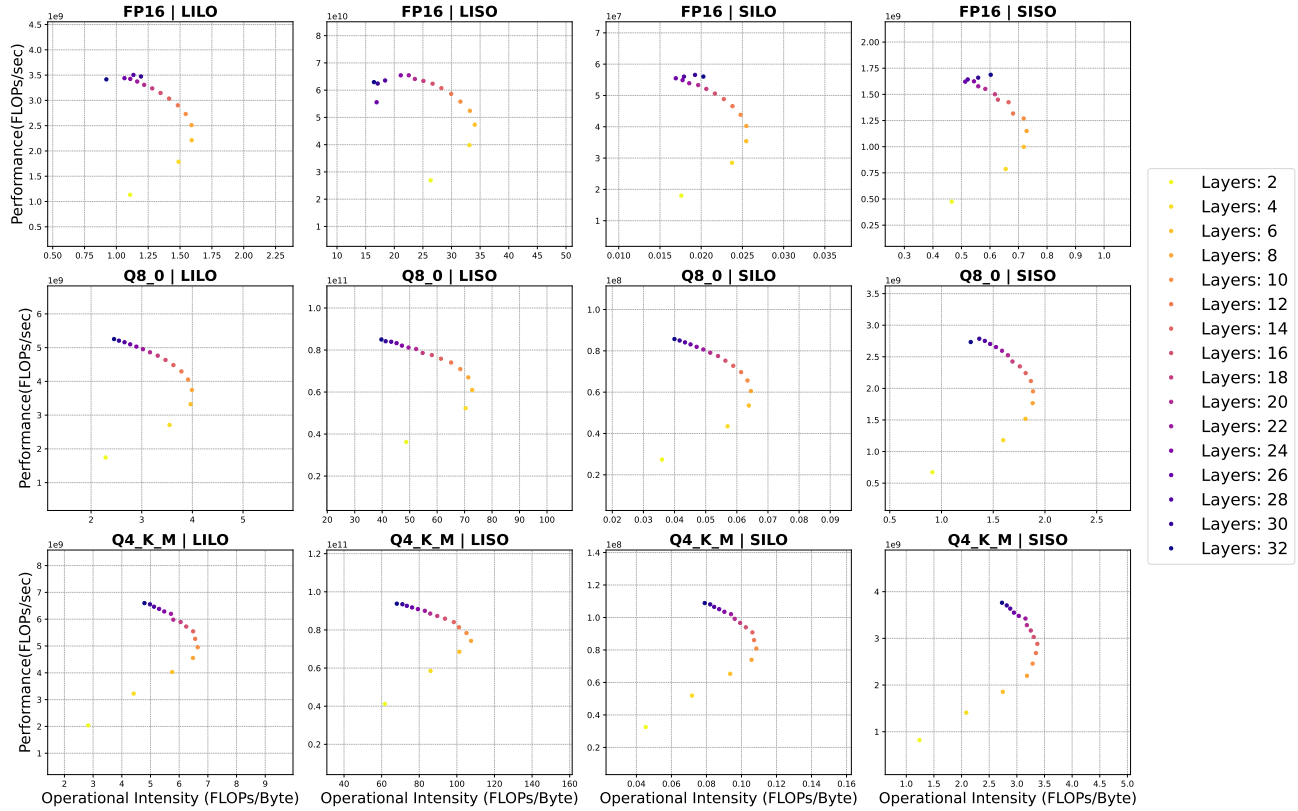
Jetson Orin Nano Super 8G - Model: PLM-Instruct


Figure 11. Layer-wise operational intensity trends for PLM-Instruct on Jetson Orin Nano Super 8G. This figure evaluates the distribution of computational intensity across Transformer layers for FP16, Q8.0, and Q4_K_M precisions. While the operational intensity typically maintains a steady profile throughout the model depth, the sharp declines observed in specific scenarios signify that the execution has encountered critical hardware bottlenecks. These straight-line drops indicate regions where the performance is heavily constrained by system resource limits, preventing the layers from sustaining their peak arithmetic intensity.

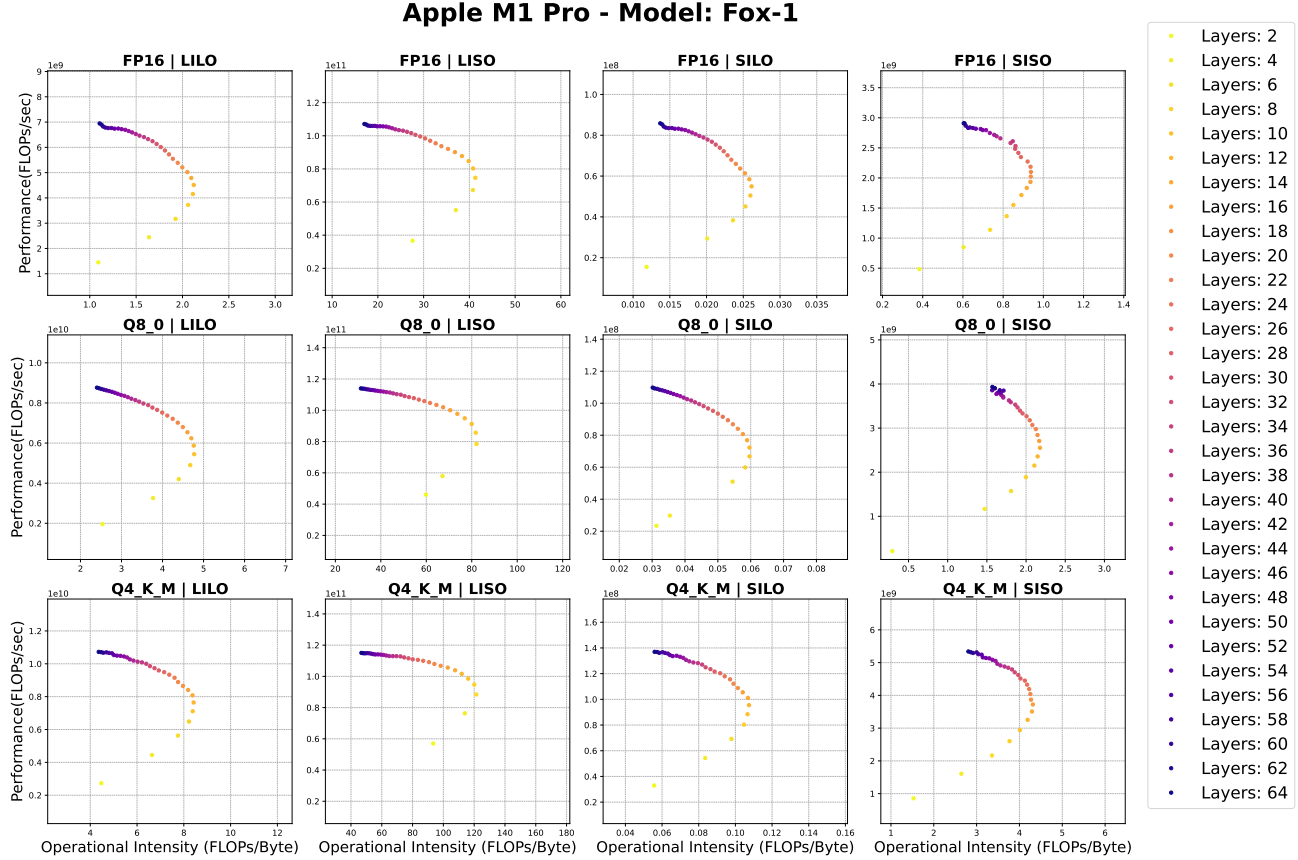


Figure 12. Layer-wise operational intensity trends for Fox-1 on Apple M1 Pro. This figure analyzes the stability of computational intensity across successive Transformer layers under FP16, Q8_0, and Q4_K_M precisions. Across the diverse inference scenarios (SISO, SILO, LISO, and LILO), the operational intensity remains remarkably constant as the layer index increases. This horizontal trend suggests that the ratio of arithmetic operations to memory traffic is intrinsically determined by the model architecture and scenario type rather than the specific depth of the layer.

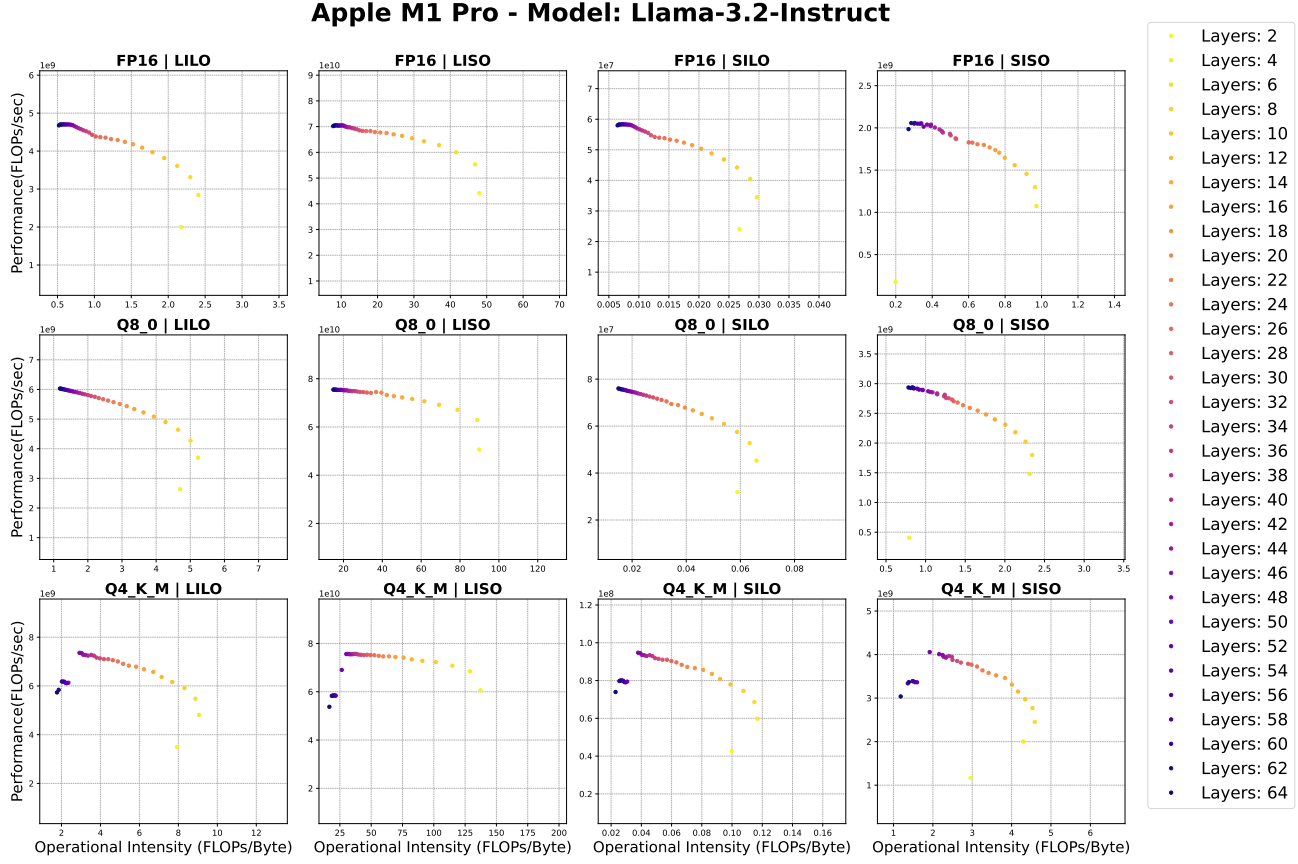


Figure 13. Layer-wise operational intensity trends for Llama-3.2-Instruct on Apple M1 Pro. The subplots illustrate the distribution of FLOPs/Byte across Transformer layers for FP16, Q8_0, and Q4_K.M precisions. While the operational intensity is generally consistent across the model depth, a sharp decline is observed in specific scenarios, signifying that the execution has encountered a critical hardware bottleneck. This transition highlights the segments where the computational efficiency is significantly hampered by data movement constraints or other resource limitations.

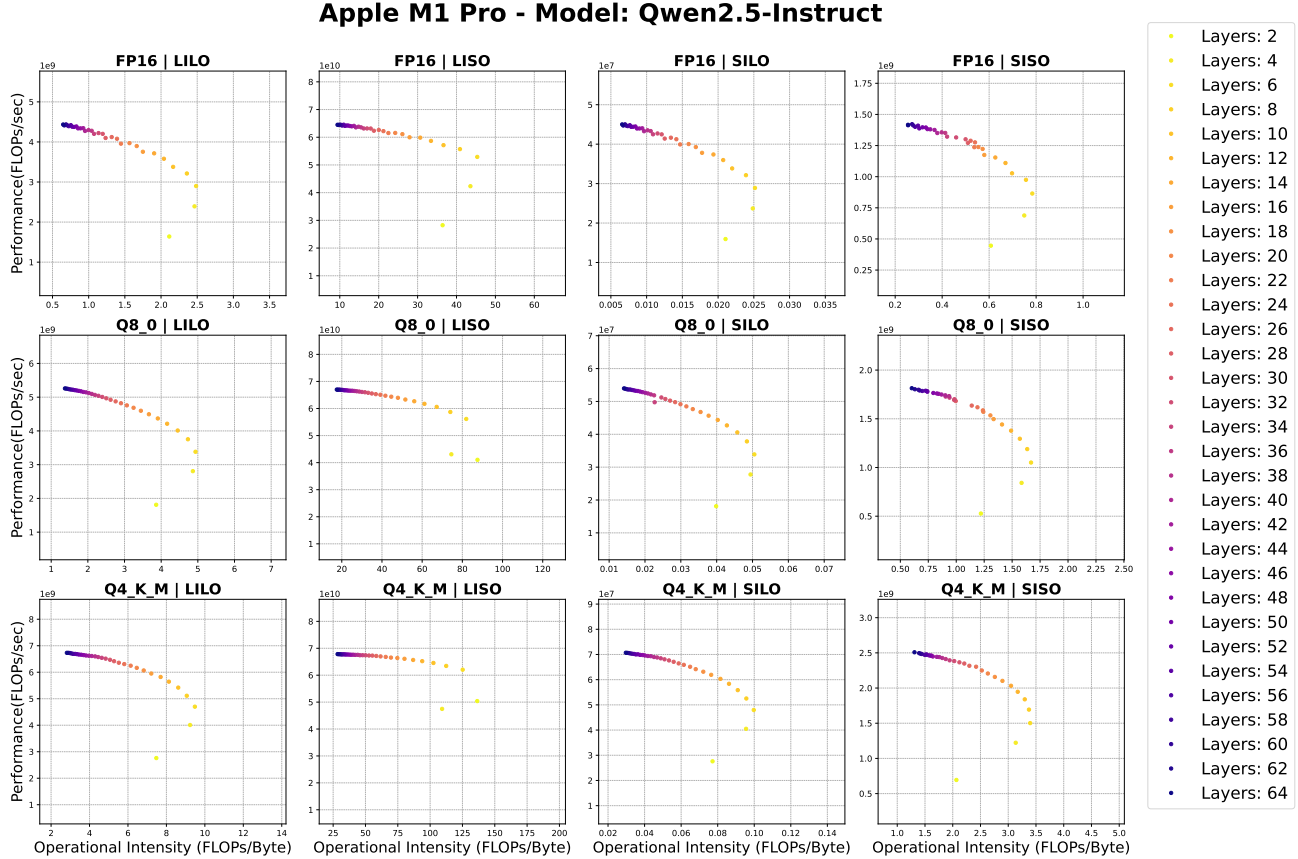


Figure 14. Layer-wise operational intensity trends for Qwen2.5-Instruct on Apple M1 Pro. These profiles characterize the layer-wise behavior of arithmetic intensity across multiple inference scenarios. The horizontal alignment of data points across the layer index confirms that the computational intensity is invariant to layer depth. This stability is maintained across all tested precisions, demonstrating that quantization shifts the absolute intensity but does not alter the uniform trend across the model’s structural hierarchy.

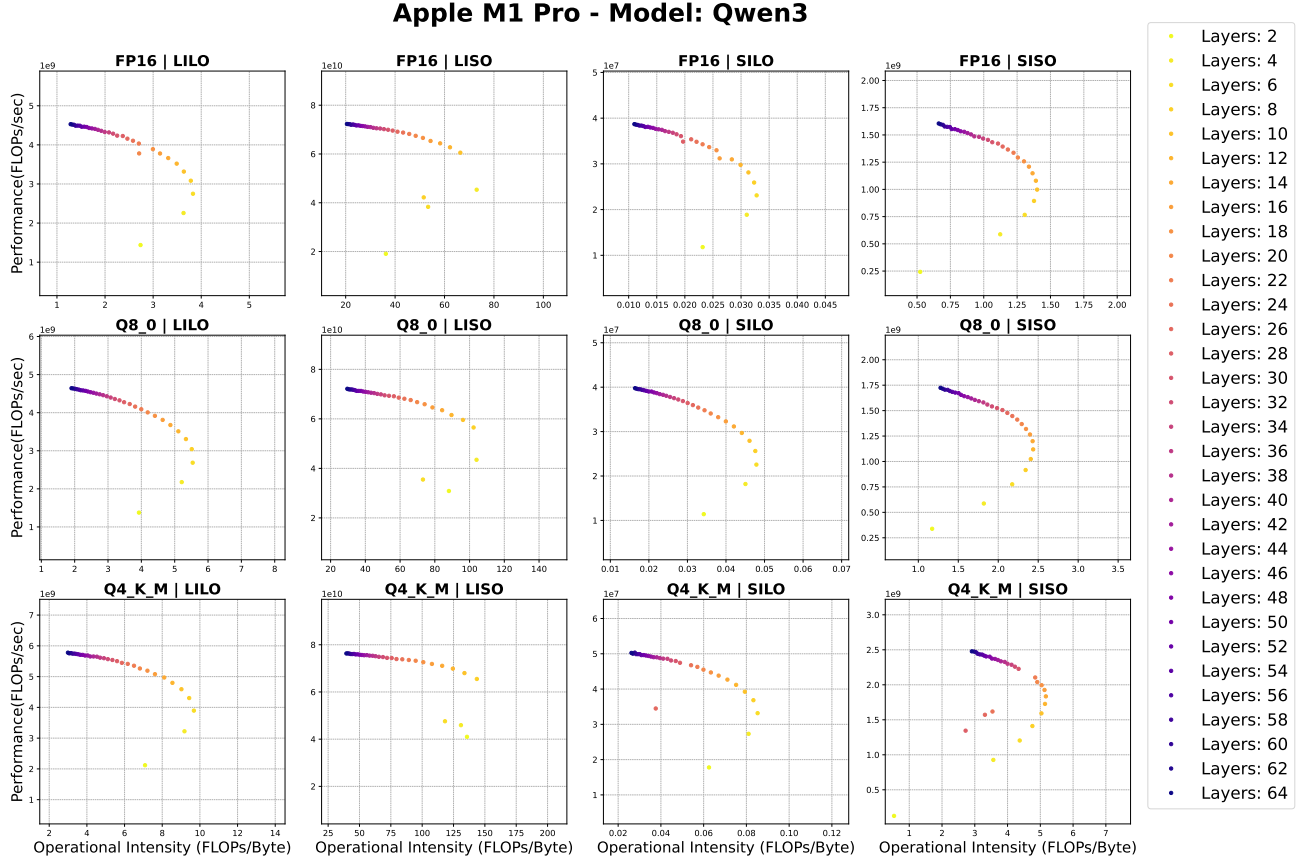


Figure 15. Layer-wise operational intensity trends for Qwen3 on Apple M1 Pro. The subplots map the operational intensity against the Transformer layer index for various precisions. Regardless of the inference workload (SISO, SILO, LISO, or LILO), the metrics exhibit a flat progression from the initial to the final layers. This trend indicates that the bottleneck characteristics, whether memory-bound or compute-bound, are shared equally by all layers within the model architecture.

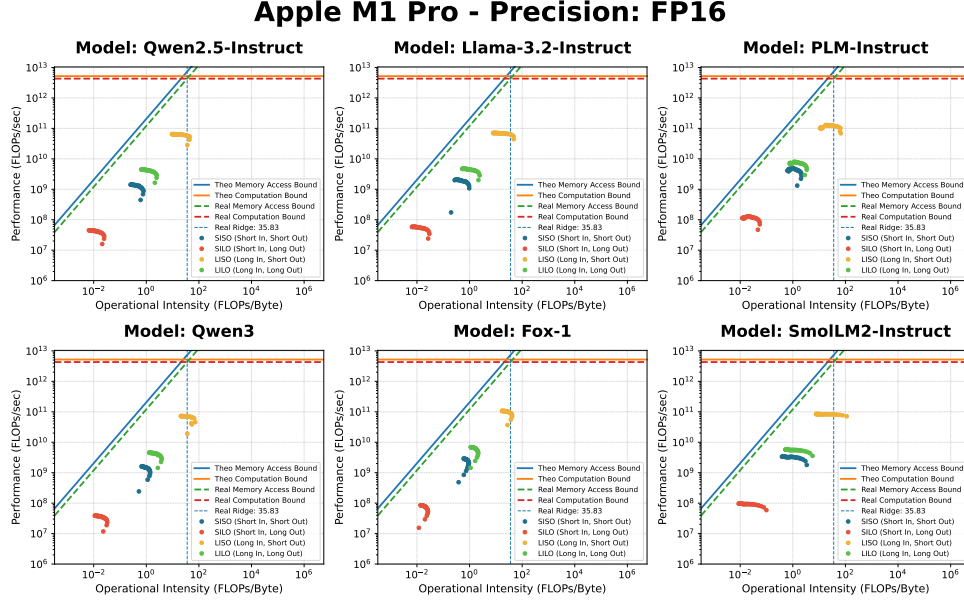


Figure 16. Performance profiles of diverse inference scenarios on Apple M1 Pro (FP16). This figure evaluates various models across four distinct operational scenarios: SISO (Short In, Short Out), SILO (Short In, Long Out), LISO (Long In, Short Out), and LILO (Long In, Long Out). The results illustrate how operational intensity (FLOPs/Byte) shifts performance (FLOPs/sec). LISO scenarios typically reach the real computation bound, while decoding-heavy SILO/LILO scenarios remain memory-bound. The hardware exhibits a real ridge point of 35.83.

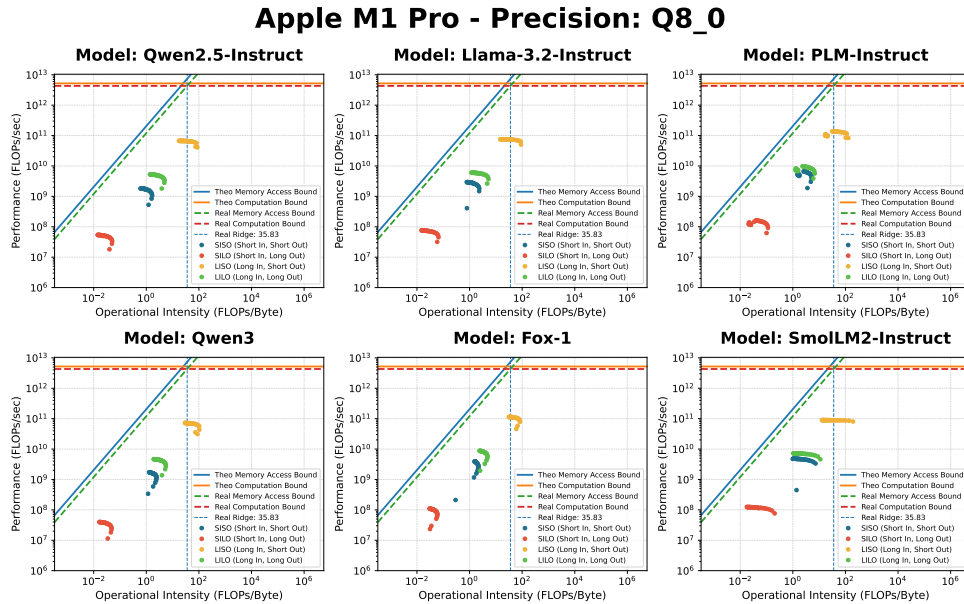


Figure 17. Performance profiles of diverse inference scenarios on Apple M1 Pro (Q8_0). This set of roofline models highlights the performance of 8-bit quantized LLMs under four characteristic workloads: SISO, SILO, LISO, and LILO. The plots demonstrate that as output length increases (SILO/LILO), the operational intensity drops significantly, trapping the performance within the memory-bandwidth-limited regime. In contrast, LISO tasks with long input sequences move toward the compute-bound ceiling. The real ridge point remains constant at 35.83.

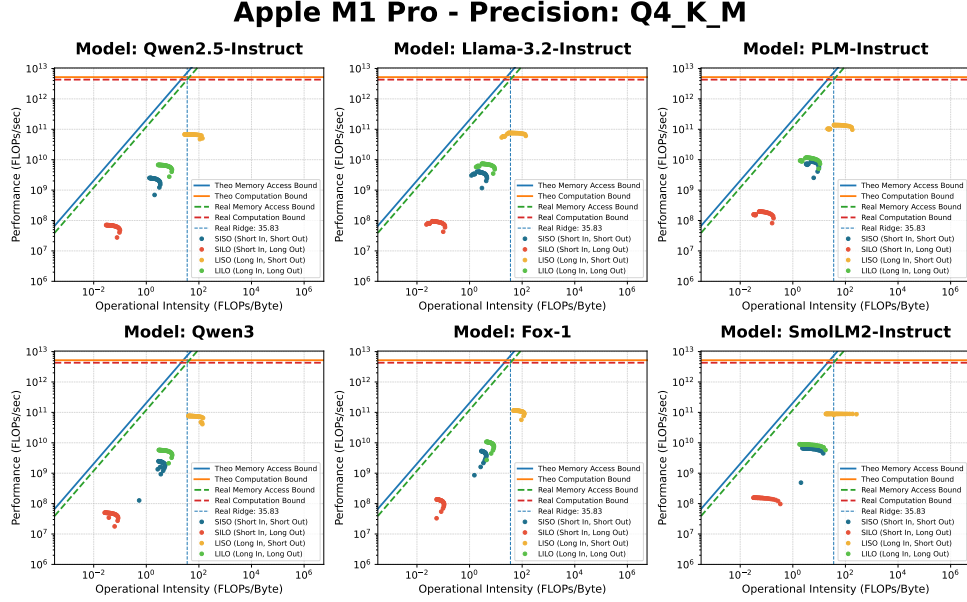


Figure 18. Performance profiles of diverse inference scenarios on Apple M1 Pro (Q4_K_M). This figure depicts the performance of 4-bit quantized models across varied input and output context lengths. By categorizing tasks into SISO, SILO, LISO, and LILO clusters, the profiles reveal the impact of quantization on arithmetic intensity and throughput. Quantization allows models to achieve higher throughput relative to the real computation bound in prefill-dominant scenarios (e.g., LISO). The dashed vertical line marks the system’s empirical ridge point at 35.83.

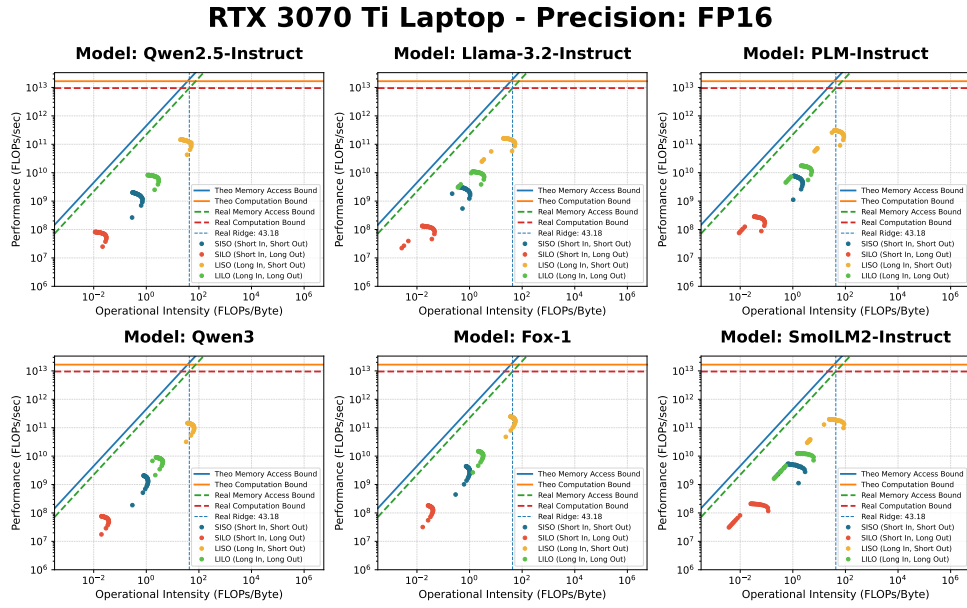


Figure 19. Performance profiles of diverse inference scenarios on RTX 3070 Ti Laptop (FP16). This figure evaluates the throughput ($FLOPs/sec$) across various models (e.g., Qwen2.5-Instruct, Llama-3.2-Instruct, and PLM-Instruct) under four distinct operational scenarios: SISO (Short In, Short Out), SILO (Short In, Long Out), LISO (Long In, Short Out), and LILO (Long In, Long Out). As operational intensity increases, tasks transition from the memory-bound region (e.g., SILO and LILO) toward the empirical computation bound, with prefill-heavy LISO scenarios exhibiting the highest arithmetic intensity. The hardware configuration exhibits a real ridge point of 43.18.

RTX 3070 Ti Laptop - Precision: Q8_0

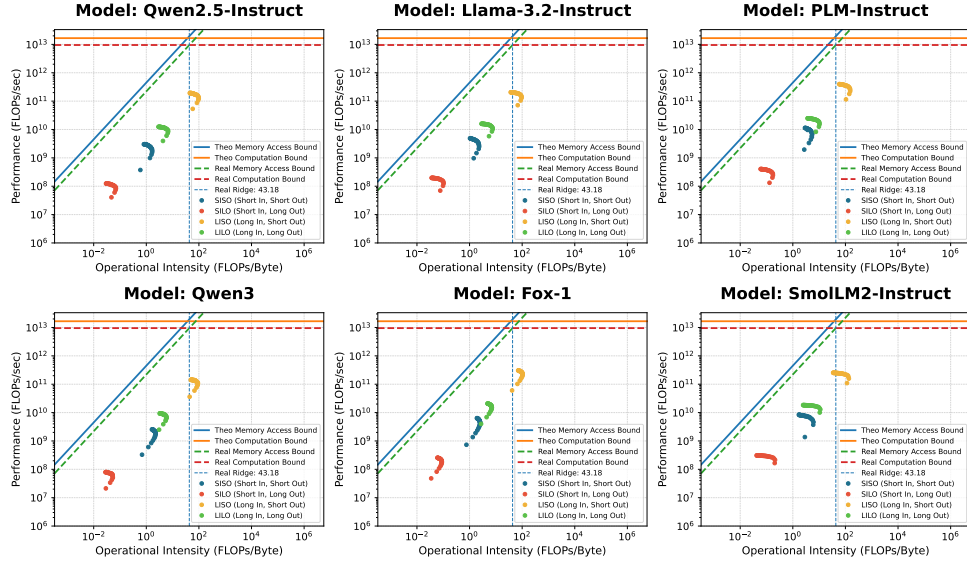


Figure 20. Performance profiles of diverse inference scenarios on RTX 3070 Ti Laptop (Q8_0). These roofline models characterize the performance of 8-bit quantized LLMs (Q8_0) under four characteristic workloads: SISO, SILO, LISO, and LILO. The results demonstrate that as output length increases (SILO/LILO), the operational intensity drops significantly, trapping performance within the memory-bandwidth-limited regime. In contrast, LISO tasks with long input sequences move toward the hardware’s empirical computation ceiling. The real ridge point is consistently identified at 43.18.

RTX 3070 Ti Laptop - Precision: Q4_K_M

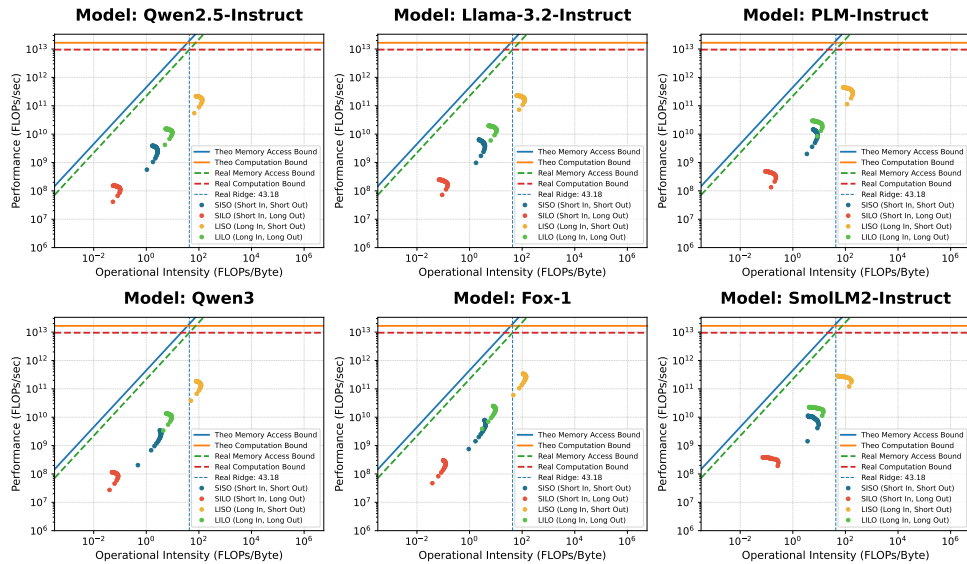


Figure 21. Performance profiles of diverse inference scenarios on RTX 3070 Ti Laptop (Q4_K_M). This set of profiles evaluates 4-bit quantized LLMs categorized into SISO, SILO, LISO, and LILO clusters to illustrate the impact of quantization on throughput across varied input/output lengths. Quantization shifts the compute-to-memory balance, allowing models to achieve higher throughput relative to the real computation bound in prefill-dominant scenarios (LISO). The dashed vertical line marks the system’s empirical ridge point at 43.18.

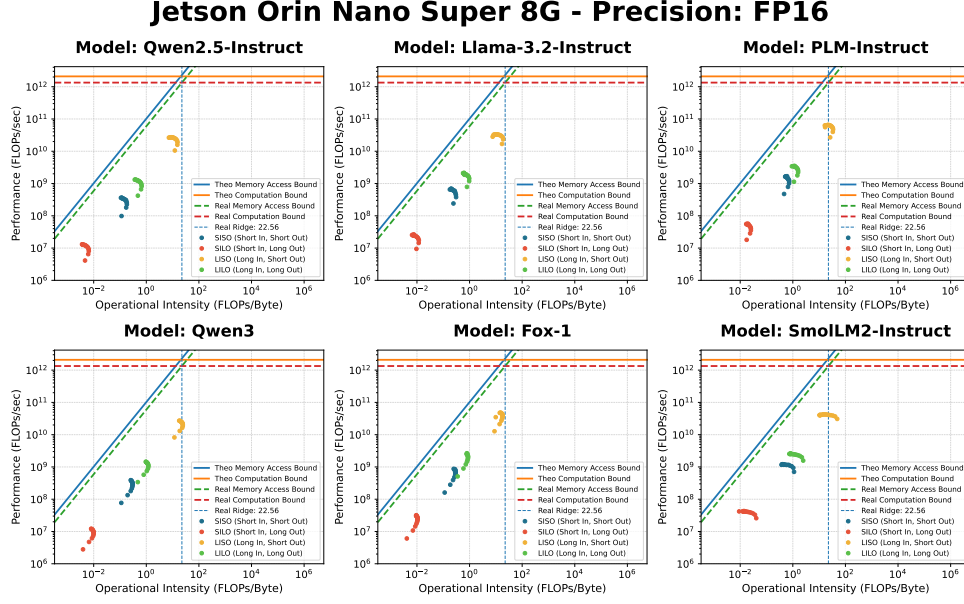


Figure 22. Performance profiles of diverse inference scenarios on Jetson Orin Nano Super 8G (FP16). This figure evaluates various models—including Qwen2.5-Instruct, PLM-Instruct, Qwen3, Fox-1, and SmoILM2-Instruct—across four distinct operational scenarios: SISO (Short In, Short Out), SILO (Short In, Long Out), LISO (Long In, Short Out), and LILO (Long In, Long Out). The subplots illustrate how operational intensity determines the achieved throughput ($FLOPs/sec$). While decoding-heavy scenarios (SILO/LILO) remain memory-bound, prefill-dominant LISO tasks approach the real computation bound. The platform is characterized by a real ridge point of 22.56.

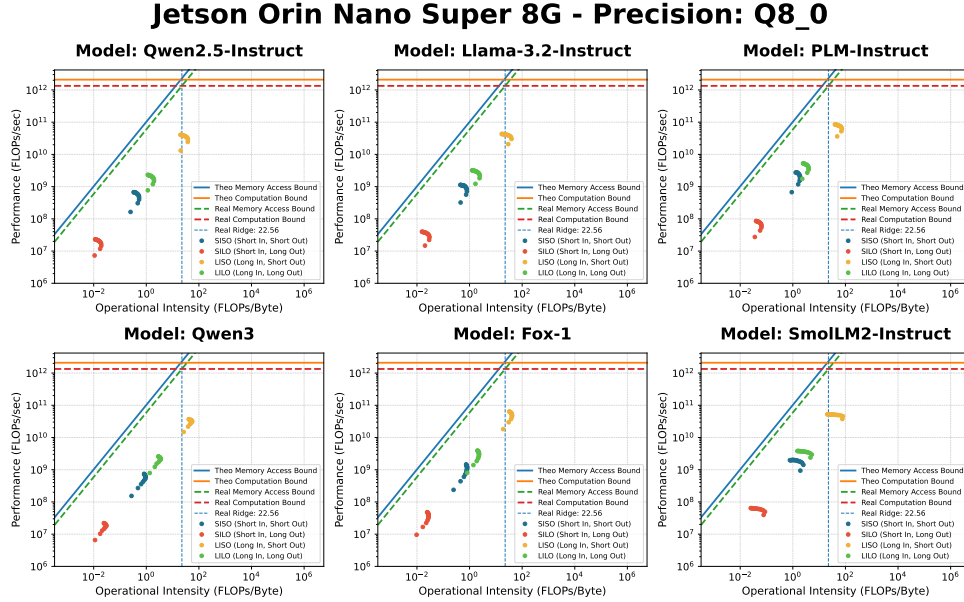


Figure 23. Performance profiles of diverse inference scenarios on Jetson Orin Nano Super 8G (Q8_0). These roofline models highlight the performance of 8-bit quantized LLMs—including Qwen2.5-Instruct, Llama-3.2-Instruct, Qwen3, Fox-1, PLM-Instruct, and SmoILM2-Instruct—under four characteristic workloads: SISO, SILO, LISO, and LILO. The plots demonstrate that as output length increases (SILO/LILO), the operational intensity drops significantly, trapping the performance within the memory-bandwidth-limited regime. In contrast, LISO tasks with long input sequences move toward the hardware's empirical computation ceiling. Consistent with the platform profile, the real ridge point is consistently identified at 22.56.

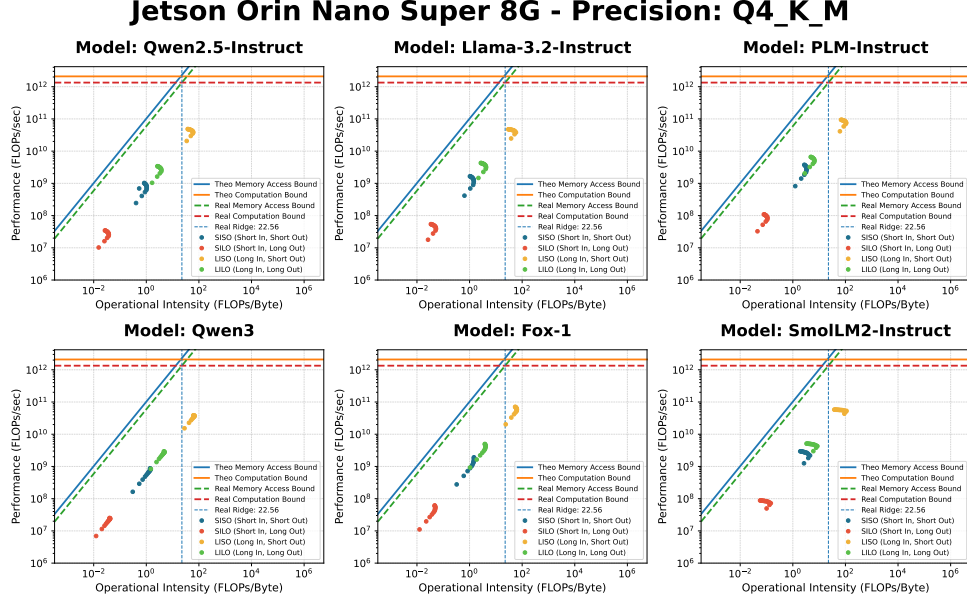


Figure 24. Performance profiles of diverse inference scenarios on Jetson Orin Nano Super 8G (Q4_K_M). This figure depicts the performance distribution of 4-bit quantized models—including Qwen2.5-Instruct, Llama-3.2-Instruct, PLM-Instruct, Qwen3, Fox-1, and SmoLLM2-Instruct—across varied input and output context lengths. By categorizing tasks into SISO, SILO, LISO, and LILO clusters, the profiles reveal the impact of quantization on arithmetic intensity and throughput. Quantization allows models to achieve higher efficiency relative to the real computation bound, especially in LISO scenarios. The vertical dashed line indicates the system’s empirical ridge point at 22.56.

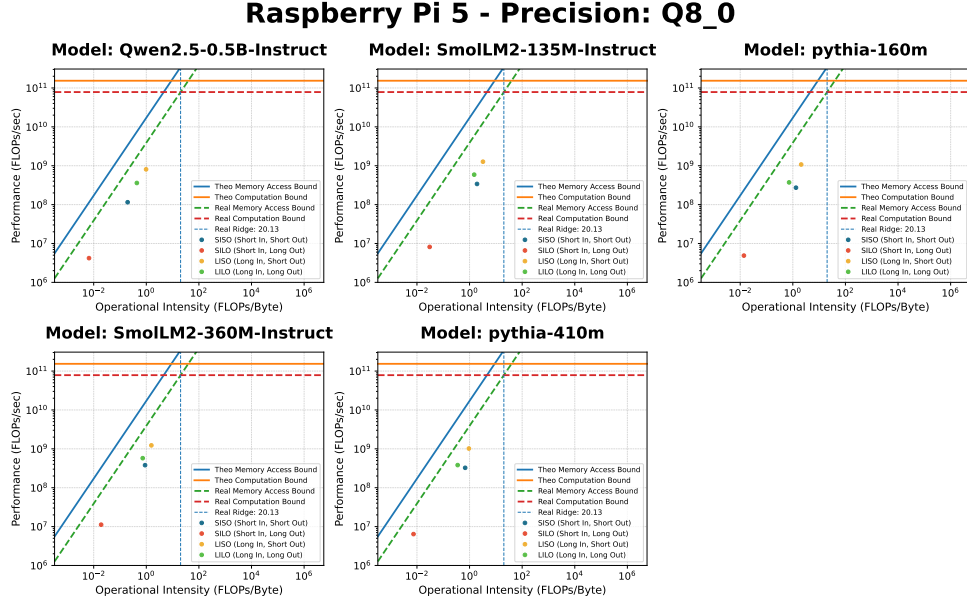


Figure 25. Performance profiles of diverse inference scenarios on Raspberry Pi 5 (Q8_0). This figure characterizes the performance of 8-bit quantized lightweight LLMs—including SmoLLM2-360M-Instruct and Pythia-410m—across four distinct operational workloads: SISO (Short In, Short Out), SILO (Short In, Long Out), LISO (Long In, Short Out), and LILO (Long In, Long Out). The subplots illustrate that in this resource-constrained environment, most scenarios are trapped within the memory-bandwidth-limited regime, particularly when output length increases (SILO/LILO). In contrast, LISO tasks with long input sequences exhibit significantly higher operational intensity, moving closer to the hardware’s empirical computation ceiling. Theoretical and real bounds are plotted with a consistent real ridge point identified at 20.13.